Title
MAGNETOTELLURIC INVESTIGATIONS AT MOUNT HOOD, OREGON

Authors
Goldstein, N.E.
Morrison, H.F.

Publication Date
1985-06-01

Lawrence Berkeley Laboratory
UNIVERSITY OF CALIFORNIA

EARTH SCIENCES DIVISION

Submitted to Journal of Geophysical Research

MAGNETOTELLURIC INVESTIGATIONS
AT MOUNT HOOD, OREGON

E.C. Mozley, N.E. Goldstein, and H.F. Morrison

June 1985

Prepared for the U.S. Department of Energy under Contract DE-AC03-76SF00098

DISCLAIMER

LBL-19547

Magnetotelluric Investigations at Mount Hood, Oregon

E.C. Mozley, N.E. Goldstein,† and H.F. Morrison†*

*Now with Naval Ocean and Research Development Activity
NSTL Station
Mississippi 39529-5004

†Earth Sciences Division
Lawrence Berkeley Laboratory
University of California
Berkeley, California 94720

June 1985

This work was supported by the Assistant Secretary for Conservation and Renewable Energy, Office of Renewable Technology, Division of Geothermal and Hydropower Technologies of the U.S. Department of Energy under Contract No. DE-AC03-76SF00098.

Magnetotelluric Investigations at Mount Hood, Oregon

*E.C. Mozley**
N.E. Goldstein†
H.F. Morrison†

*Now with Naval Ocean and Research Development Activity
NSTL Station, Mississippi 39529-5004

†Earth Sciences Division
Lawrence Berkeley Laboratory
University of California
Berkeley, California 94720

ABSTRACT

Magnetotelluric data, with both electric and magnetic field references for noise cancellation, were collected at accessible locations around and as close as possible to the Mount Hood andesite-dacite volcano. The purpose of the study was to identify and map conductive features and to relate them to the thermal regime of the region. Several conductors could be discerned. The shallowest, at a depth of around 500 m below the surface, was identified as a flow of heated water moving away from the summit; the deepest (~50 km) might be a melt zone in the upper mantle. Of particular interest is an elongate conductor that strikes N10° W and extends from a depth of 12 km down to 22 km. Because the conductor strike is close to the trend of the chain of Cascade volcanoes and because of the high conductive thermal gradients reported for the area, this feature was initially believed to be a zone of partial melt following the volcanic axis. However, because no teleseismic P-wave velocity anomaly has been found, the cause of the conductor is more problematic. While the existence of small zones of melt cannot be ruled out, it is possible that the conductor is caused by a large volume of intensely deformed rocks with brine-filled microfractures.

INTRODUCTION

As part of a combined effort of the Department of Energy, the U.S. Geological Survey, the Forest Service of the U.S. Department of Agriculture, and the State of Oregon to assess of the geothermal resource potential of the Cascades, a number of geologic, geochemical, and geophysical investigations were conducted around Mount Hood, Oregon (Williams et al., 1982). This area was chosen for several reasons: the generally good road access around the Pleistocene-Holocene volcano, the relatively large number of nearby potential users of geothermal energy for space heating, and the various geothermal manifestations, such as fumaroles at the summit and warm springs on the south flank.

Magnetotelluric (MT) methods were used to search for electrical conductivity anomalies that might be caused by melt or partial melt zones in the crust beneath the volcano. This paper describes the processing and interpretation used to discern several conductivity anomalies associated with the volcano and to determine their relation to other geophysical anomalies and to geologic models.

Law et al. (1980) analyzed geomagnetic variations observed at stations on an east-west line 120 km north of Mount Hood. They fitted the variations to a line source of current at a depth of 17 km and aligned with the trend of the High Cascades. They concluded that the conductor might be the effect of a plate boundary. Stanley (1984) analyzed the results of several lines of magnetotelluric stations running east-west across the Cascades in Washington. Although the station separations were too large to elucidate hydrothermal-magmatic systems associated with the Cascades, he showed that the geomagnetic variation anomaly can be explained in terms of a large, closed current loop. Ocean electric currents channeled into Puget Sound persist to the southeast, flowing through the conductive sediments of the Puget Lowland and thence into a possible deep conductor beneath the High Cascades before returning to the Pacific Ocean. The specific question of whether a deep conductor can be discerned beneath Mount Hood by means

of MT soundings, and the possible relation of such a conductor to melt zones, is discussed in this paper.

GEOLOGIC SETTING

Mount Hood is one of the major Pleistocene-Holocene composite volcanoes of the High Cascade chain, which extends from northern California into southern British Columbia (Fig. 1). The geology has been discussed and reviewed by many workers, including Wise (1968, 1969), Crandall (1980), and Priest (1982), and will be only briefly reviewed here. The volcano consists of approximately 180 km^3 of dominantly andesitic flows and pyroclastic debris (Fig. 2). Most of the cone formed less than .73 Ma ago, because no flows with reversed magnetization have been found (Wise, 1969; Crandall, 1980). Potassium-argon ages from two augite andesite flows west of the volcano range from .57 to .35 Ma, roughly the same age range as obtained for the olivine andesites that erupted from three major satellite vents on the north flank (Keith et al., 1985). Following the Fraser Period of glaciation, which began 15,000 years ago, there were three principal periods of dacitic volcanism (Crandall, 1980). The earliest occurred 12,000 to 15,000 years ago when mud and pyroclastic debris flowing down the flanks filled glacial valleys and dacitic domes were extruded near the summit. The second period, 1500 to 1800 years ago, was similar to the first but smaller in magnitude. Volcanic debris flowed southward through a breach in the wall of the summit crater. The final major activity occurred only 200 to 300 years ago with the extrusion of a prominent dacitic plug at the summit (Crater Rock) and the ejection of a large volume of debris into the Sandy River and White River drainages (Crandall, 1980). Small pumice eruptions at the summit were witnessed in 1859 and 1865 (Crandall, 1980). Fumarolic activity occurs today at about 20 vents around Crater Rock, indicating that the plug is still cooling (Wise, 1968).

Mount Hood developed on a platform of folded and thrust-faulted Miocene Columbia River basalts, late Miocene tholeiitic basalts to calc-alkaline andesites intruded by

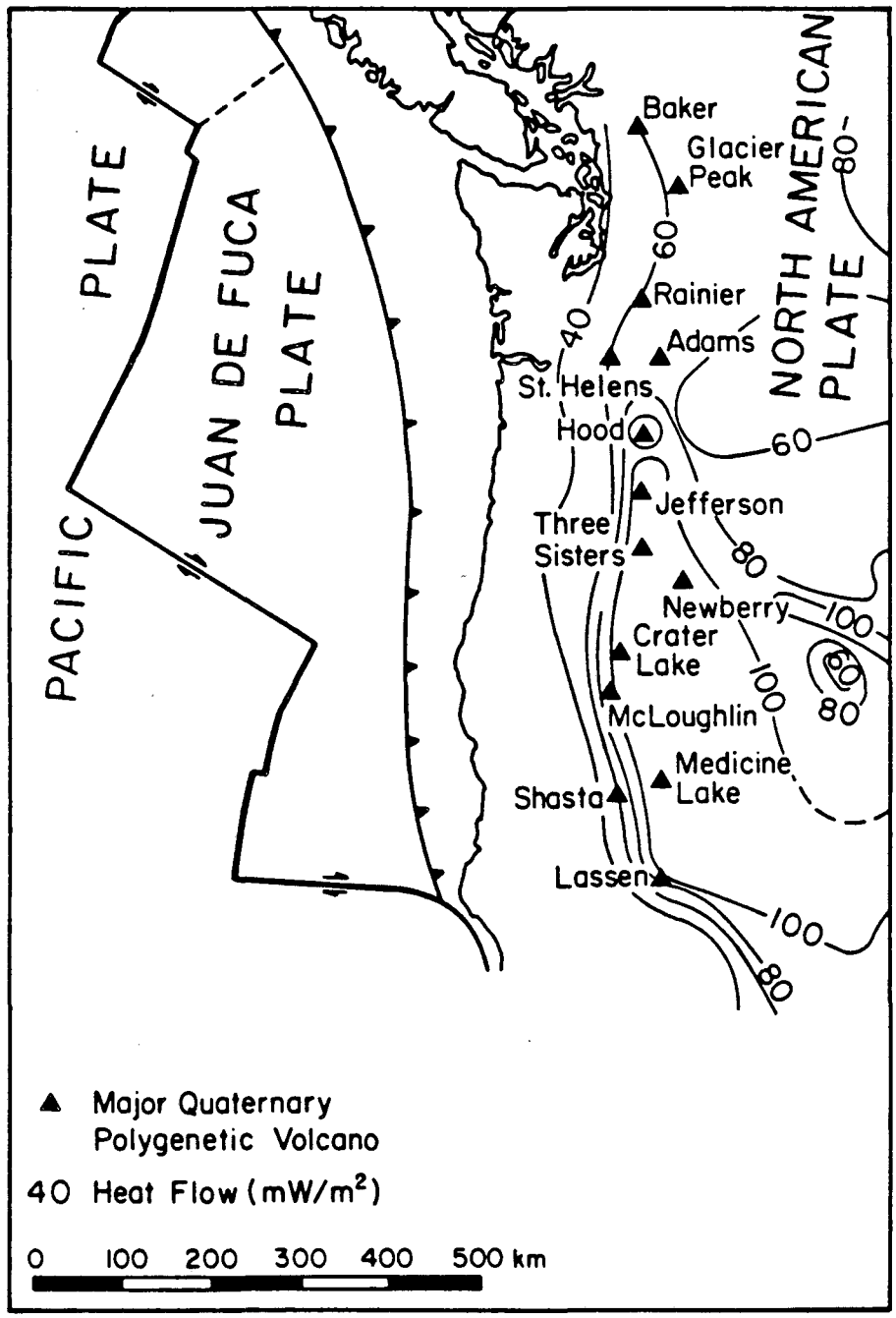

Figure 1. Tectonic structure, location of volcanoes, and generalized heat flow pattern for the Cascade Range (after Bacon, 1981; Blackwell, 1978; Blackwell et al., 1978; Black, 1983).

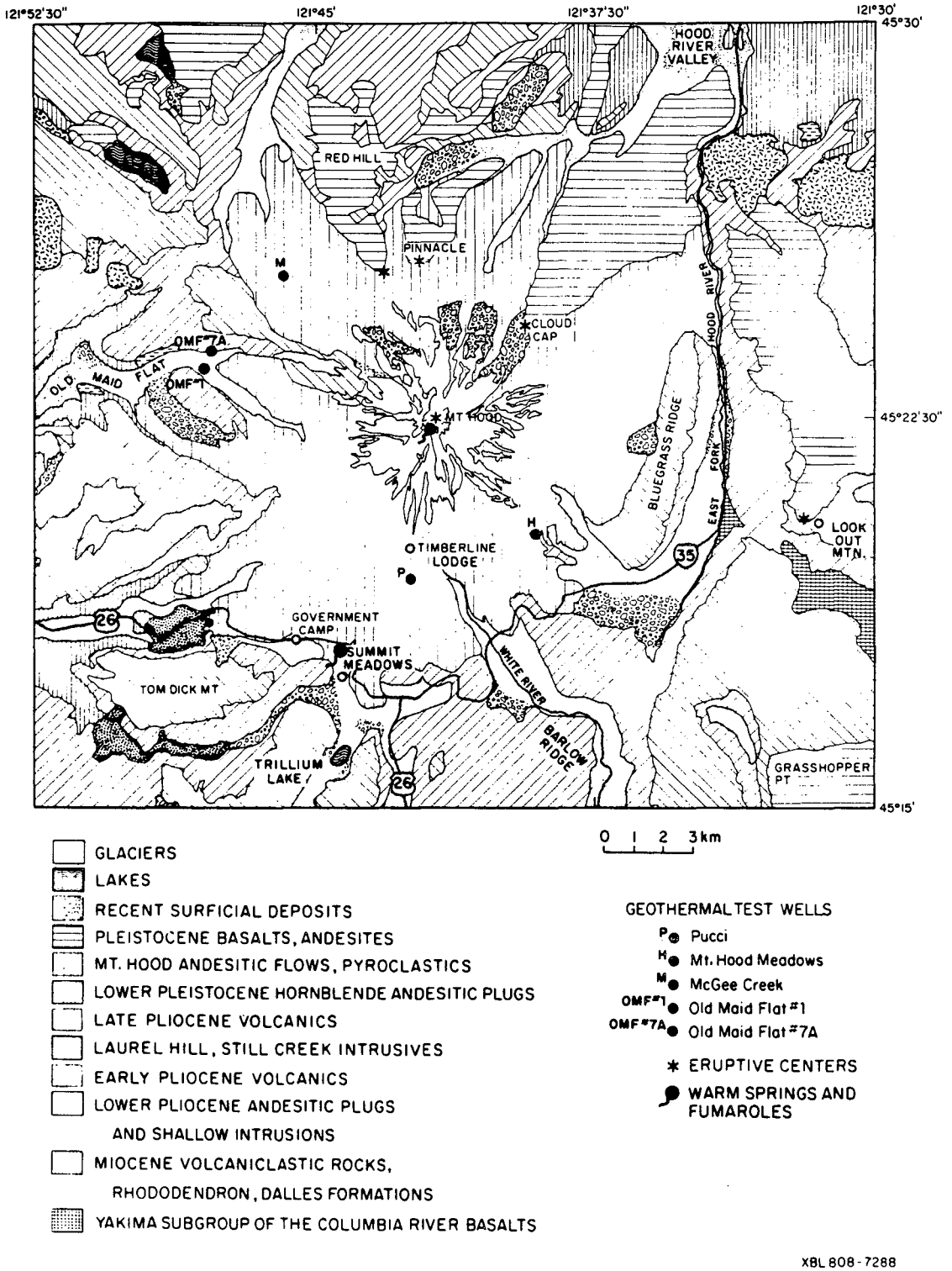

Figure 2. A simplified geologic map of the Mount Hood area (after Wise, 1969), showing locations of some geothermal test wells.

quartz diorite plutons (also late Miocene), and Pliocene andesites and dacites. The Laurel Hill (8 Ma) and Still Creek (11 Ma) intrusives south of Government Camp are two of the better exposed remnants of the quartz diorite plutons. There is evidence that Mount Hood covered remnants of several slightly older Holocene tholeiitic to calc-alkaline volcanoes, one of which was exhumed by the Sandy Glacier on the west flank (Wise, 1969) and recently dated at 1.1 to 1.3 Ma (Keith et al., 1985).

Allen (1966) reported that the volcano lies within a graben bounded on the east by the north-south Hood River-Green Ridge faults (along the East Fork of the Hood River) and on the west by numerous, unnamed faults recognized by Thayer (1937) and Callaghan (1933). On the basis of gravity data, Couch and Gemperle (1979) also find evidence for a graben. Williams et al. (1982) report that the graben is probably a local extension of the graben mapped in other parts of the High Cascades, that it is asymmetric with no apparent offset on the west, and that it developed as a result of magma withdrawal and subsidence. However, Priest et al. (1982) found evidence for a northwest-trending fault, located a few kilometers west of Mount Hood, that shows substantial down-to-the-east displacement. Aeromagnetic data from the Mount Hood area also suggest a smaller subsidence block associated with the volcano (Williams et al., 1982).

PREVIOUS GEOPHYSICAL STUDIES

Gravity, aeromagnetic, seismic, and electromagnetic studies have been carried out by various workers to assess the geothermal potential of the Mount Hood area and to test the theory that a magma body exists beneath the volcano. Weaver et al. (1982) found no evidence from a teleseismic P-wave delay study for a velocity anomaly that could be associated with a large ($>$ 3 km diameter), shallow magma body.

The large magnetic anomaly resulting from the cone, mainly a topographic effect, masks the effects of magnetic sources within and beneath the cone (Flanagan and

Williams, 1982). Removing the magnetic effects of the cone, they found evidence in the residual anomaly for smaller, older cones buried beneath the flanks of the volcano. Magnetic lows are believed associated with the less magnetic quartz diorite stocks.

High-pass-filtered Bouguer gravity measurements revealed a number of small gravity highs that could be due to density variations within the volcanics or concealed stocks and cupolas (Couch and Gemperle, 1979). A gravity anomaly at the summit was modeled as a dense cylindrical core (Couch and Gemperle, 1979; Williams and Keith, 1982) that presumably represents a neck-type intrusive.

Controlled-source electromagnetic and magnetotelluric (MT) surveys around the volcano (Goldstein et al., 1982) focused mainly on the near-surface environment and verified the existence of shallow conductors beneath the flanks of the volcano. These conductors probably consist of porous and permeable volcanic units saturated with the outflow of meteoric water (snowmelt) heated at the summit (Wollenberg et al., 1979).

MODELS FOR MAGMA BENEATH HIGH CASCADE VOLCANOES

The High Cascades and the remnants of older and partially exposed volcanoes are commonly believed to have resulted from subduction of the Juan de Fuca plate beneath the North American plate (Fig. 1). Blackwell et al. (1978) show that the high heat flow in the High Cascades and the much lower heat flow in the Western Cascades is easily explained in terms of the subduction model. However, petrologic interpretations by White and McBirney (1978) suggest that subduction may have contributed to the formation of the High Cascades but was not the only tectonic process involved. Although there remains a long-lived thermal anomaly associated with subduction, petrologic evidence shows that active subduction may have ceased long ago. Priest et al. (1981) argue that the shift to more mafic volcanism in the southward direction from Mount Hood may be the result of the increasing influence of extensional deformation that began in late Miocene (10 to 8 Ma ago) a time that correlates with the onset of Basin and Range

deformation and a change in the plate-tectonic environment (Atwater, 1970; Zoback and Thompson, 1978; Davis, 1981). Subordinate crustal extension is consistent with Hildreth's (1981) conceptual model for an andesitic-dacitic volcanic cluster.

Although there are 25 temperature-gradient drill holes within a 20-km radius of the summit, none is close enough to the summit to detect the thermal effects from a neck-type heat source. However, the fumaroles around Crater Rock indicate that such a source should exist. Steele et al. (1982) find that although the available data on the conductive gradient do not support the presence of a large, subvolcanic magma chamber (i.e., one whose top is < 3 km and whose radius is 2 to 3 km), a deeper melt zone is possible. White (1980) estimated that the most recent eruptions, those in the last 10,000 years, may have originated from a magma at a depth of 8 to 10 km. This is consistent with one model for the 1980 Mount St. Helens eruption, in which the magma is believed to have evolved from a relatively small (10 to 20 km^3) zoned melt at a depth of 7 to 9 km (Scandone and Malone, 1985). The Mount St. Helens chamber may have had a diameter of 1.5 km, but the magma ascended via a conduit only 50 m in radius (Scandone and Malone, 1985; Carey and Sigurdsson, 1985). It is estimated that eruption recurrence rates of greater than 1 per 1000 years, such as at Mount Hood, will keep the conduit at or above the solidus temperature. This condition is required for repetitive intrusions of relatively small, high-viscosity magmas at the same location--typical of many andesite-dacite volcanoes.

Arguments for a deeper, long-lived magma source beneath the Mount Hood area are based on temperature-gradient measurements. A magma depth of 12 to 14 km is obtained by making topographic corrections and then extrapolating the local conductive gradient of 65 °C/km measured in the Miocene rocks (Steele et al., 1982). As we show here, this depth is in good agreement with the depth to a north-south-trending conductor beneath the volcano.

DATA ACQUISITION AND PROCESSING

The MT data were obtained by a commercial contractor in accordance with the remote reference scheme introduced by Gamble et al. (1979) and now widely used in MT surveys to reduce the effects of statistically uncorrelated signals, such as random noise in the recorded magnetic and electric fields. Each instrument setup consisted of a tensor MT base, two remote telluric stations, and a remote magnetic station. Figure 3 shows the station arrays; cluster locations were selected on the basis of road access and our desire to get as close as possible to the summit. Details of the data-acquisition system were reported by Mozley (1982) and by Goldstein et al. (1982). Impedance estimates were obtained at the telluric sites on the assumption that the magnetic fields are uniform across each instrument cluster, a distance of approximately 4 km (Hermance and Thayer, 1976). Because this assumption was shown to be incorrect in the presence of 2-D and 3-D inhomogeneities when measurement separations are large (Stodt et al., 1981), the assumption was tested by acquiring six stations as both remote telluric and as full tensor MT stations. Only at one measurement site was there a significant amount of distortion due to lateral variations in the magnetic field, and the distortion was limited to the higher frequencies, $>.5$ Hz. Therefore, we can safely assume that the remote telluric stations provide data for valid analysis in the lower frequency range.

Clusters 1 and 2 were located at Cloud Cap, 3 to 5 km from the summit, on the flow from one of the three olivine-andesite satellite vents on the northern flank of the main cone. Clusters 3 and 4 extend in an east-west line across the East Fork of the Hood River; they were so located to determine whether a structural discontinuity related to the High Cascade graben could be detected. Clusters 5 and 6 follow the White River drainage; these sites were selected to delineate an anomalous conductor south of Timberline Lodge. Cluster 7, west of the volcano, was located in the Old Maid Flat area where two holes were later drilled These holes provided constraints on our MT interpretation. In addition to these clusters, we occupied a number of stations on the south flank, from

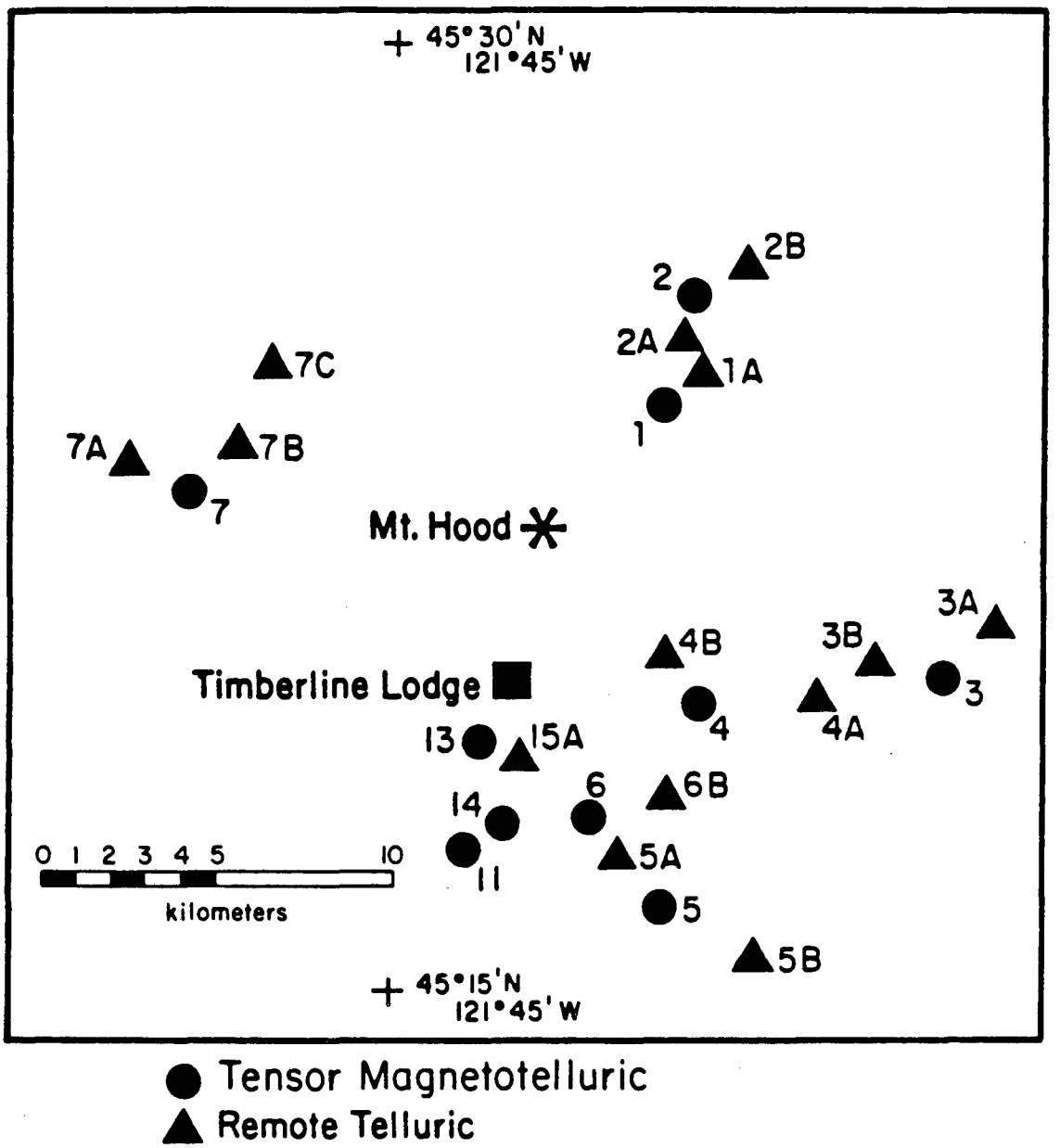

Figure 3. Magnetotelluric stations in the Mount Hood area that provided data for the analysis reported here.

Timberline Lodge southward through the only warm springs (Swim Springs) in the area. Figure 3 shows only the stations with data good enough to interpret. Data from several stations on the south-southwest side of the mountain were of poor quality due to cultural noise associated with the ski resort.

Remote reference processing was done on all edited and smoothed data (Gamble et al. 1979; Mozley, 1982). These data were Fourier transformed and stacked in the frequency domain, then averaged over constant Q windows. Impedances were calculated using both remote magnetic and remote telluric data. The impedance tensors were numerically rotated to determine the principal directions of electrical conductivity, and both the apparent resistivity and phase spectra were calculated for the principal directions (Vozoff, 1972). In general, the calculated spectra were independent of the reference, but the magnetic reference provided a slightly more reliable impedance estimate because the electric fields were characterized by a larger noise component than the magnetic fields.

The rugged terrain in the survey area provided a potentially troublesome source of bias for the impedance tensor. An approximate correction procedure was implemented to evaluate the effect of the topographic distortion at each measurement location (Mozley, 1982). This procedure utilized a dc forward modeling scheme which calculated the electric field over the digitized terrain for two plane wave source polarizations. These two solutions provided a distortion matrix which was used to transform the measured tensor impedances. This transformation provided apparent resistivities which were free of topographic effects. Only stations 3 and 3A, which were located in an area of steep terrain, required a significant correction.

DATA INTERPRETATION

One-dimensional interpretations were made at all the stations for which this type of analysis seemed reasonable. Soundings on the northeast flank of the volcano (clusters 1 and 2) were particularly amenable to 1-D inversions; impedance strike directions were similar at all stations, and there were only slight offsets in the apparent resistivities calculated from the off-diagonal terms of the impedance tensors. The impedance data for this cluster were rotated into the same principal direction on the basis of the average strike direction at all frequencies and at all stations in the clusters. This direction, associated with the x-directed component of the electric field in the Z_{xy} impedance term, was N80°E. Figure 4 shows a 1-D inversion of the two off-diagonal impedances at one of the stations; calculations were made using the parameterized technique developed by Jupp and Vozoff (1975). Because the data do not fit a 1-D earth model at the longer periods, conductivities at depths >3 km are regarded as speculative. Figure 5 shows a composite section of shallow resistivities at clusters 1 and 2. The shallow conductive zone at a depth of 500 m sub-surface was corroborated by controlled-source EM soundings (Goldstein et al., 1982) and may be due to a flow of warm water away from the summit. There are no drill holes in this area, however, to confirm the electrical model.

Simple 1-D inversions were also made at stations on the south flank of the volcano. Although the data from these stations are of poor quality, which limited impedance estimates to periods longer than 0.1 s, they do indicate a conductive layer (5 to 20 ohm·m) at a depth of 300 to 700 m. This layer is probably a warm water aquifer associated with the pyroclastic debris of one of the more recent eruptions. Even though temperature-gradient wells near Timberline Lodge supported this interpretation, we carried out some 3-D simulations using a modified version of the hybrid modeling scheme introduced by Scheen (1978) and described by Pridmore (1978) and Lee et al. (1981). The dark stippled region in Figure 6 outlines an area where the apparent resistivity polar diagrams for the bandwidth 0.01 to 0.001 Hz indicate a north-south polarization of the electric field

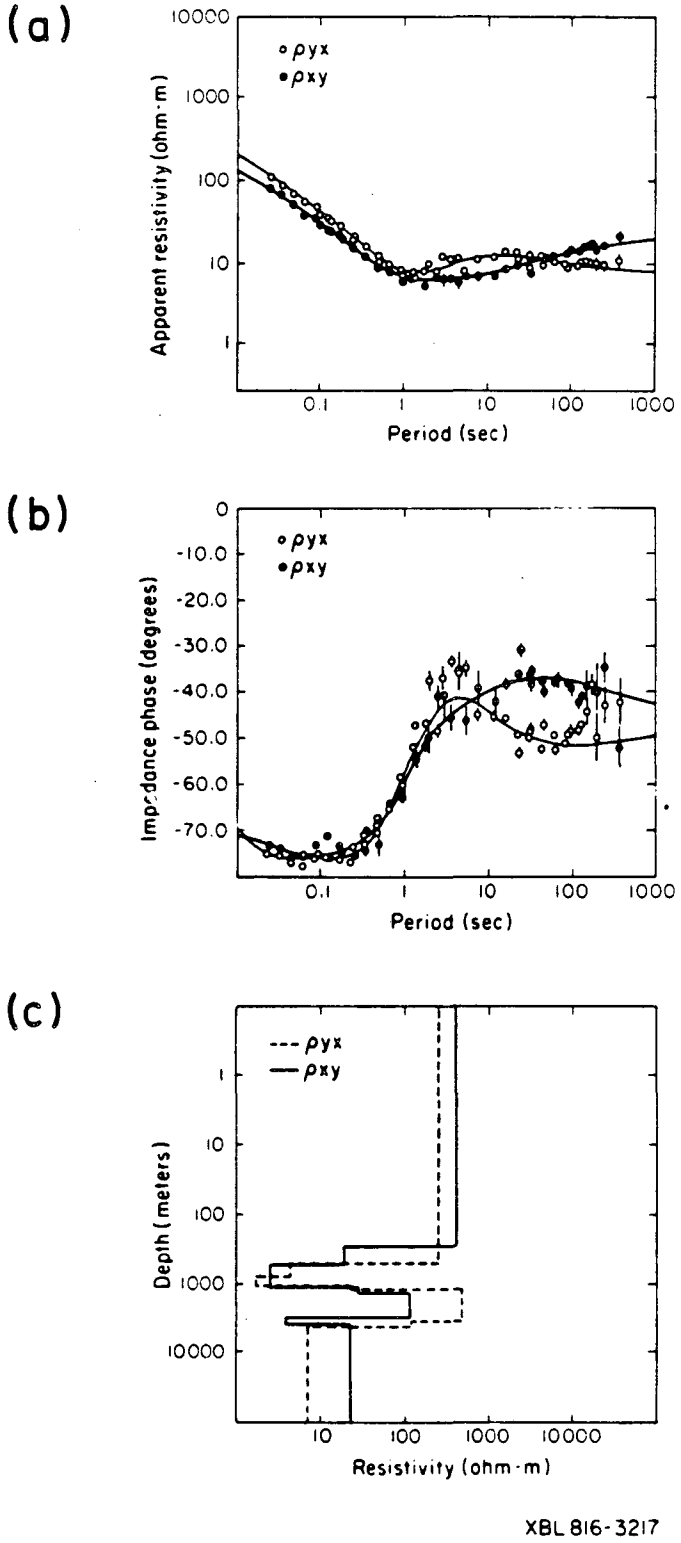

Figure 4. An example of 1-D inversions of the off-diagonal impedance elements for site 1. The smooth curves in (a) and (b) are the calculated amplitude and phase spectra for the layered model in (c).

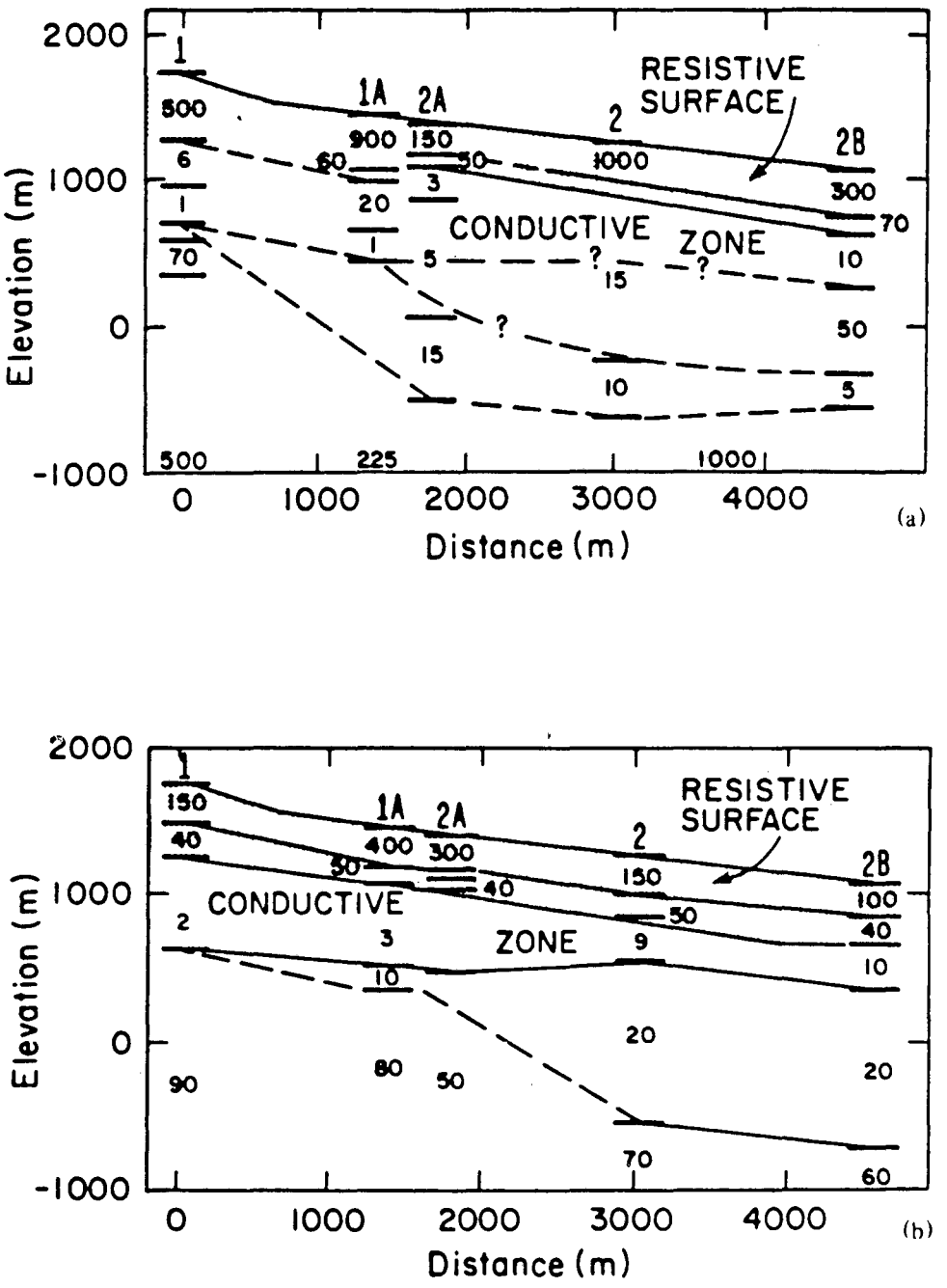

Figure 5. Subsurface resistivity distributions based on 1-D inversions of MT data from clusters 1 and 2. The upper section is for impedance element Z_{xy} associated with the electric field oriented N80°E. The lower section is for impedance element Z_{yx} associated with the electric field oriented S10°E. Units are ohm·m.

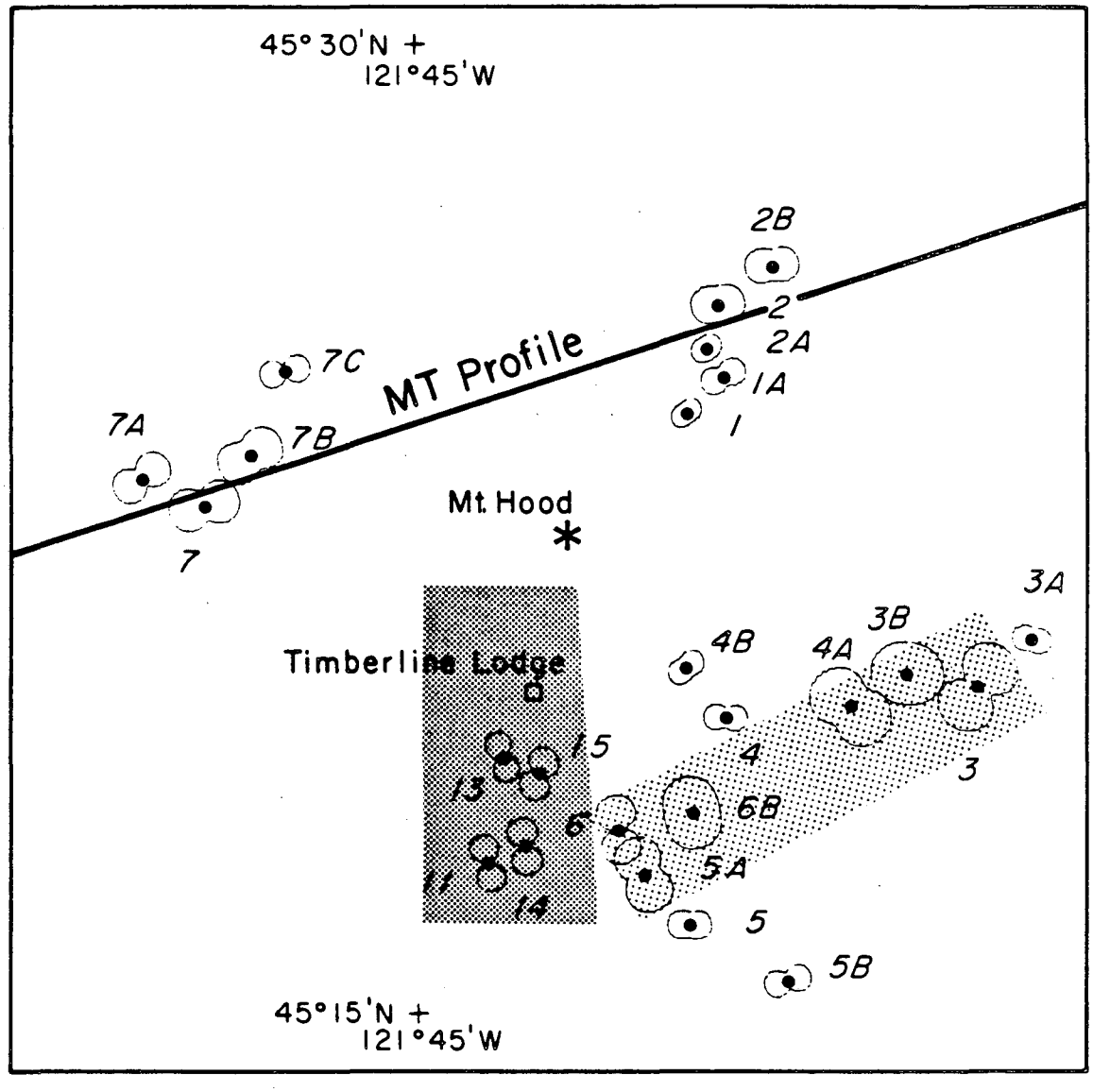

Figure 6. Apparent resistivity polar diagrams for the field data averaged over the bandwidth 0.001 to 0.01 Hz. The dark stippled region is the approximate location of what appears to be a near-surface conductor on the south flank of the volcano. The lightly stippled region indicates the probable region of a near-surface resistive body. The MT profile line is perpendicular to the strike of the deep conductor (not shown) as determined from analyses of both the apparent resistivity tensor and residual phase.

due to the shallow conductor. These data may be compared with the calculated polar diagrams for an embedded 3-D conductor (10 ohm·m) at a depth of 500 m (Fig. 7). In the numerical case, E-field parallel-to-strike produces apparent resistivities over the conductor that are about twice as large as those with the E-field perpendicular-to-strike. However, the simple one-body model does not yield the figure-eight polar diagrams observed in the dark stippled area of Figure 6. The next simulation considers a two-body model: a shallow conductor underlain by an elongate, orthogonal resistive body, as shown in Figure 8. The polar diagrams now take on the figure-eight shape at points over the conductor, demonstrating that the underlying resistive structure enhances the polarization effects. By varying model parameters, we might have been able to improve the fit, but this was not done because of the high cost of the calculations and because of the code is limited, numerically, to models with low resistivity contrasts and simple geometries.

The underlying resistor seems to approach the surface on the southeast side of the volcano, in the vicinity of clusters 3 to 6 (Fig. 6). This is evidenced by the large amplitudes of the apparent resistivity polar diagrams and is supported by the calculated polar diagrams for the shallow resistive 3-D body shown in Figure 9. This interpretation was supported by the complex tippers and associated induction arrows obtained at all sites where three-component magnetic data were acquired. These transfer functions were bimodal in character with dominant peaks in amplitude occurring near frequencies of 2.0 Hz and .03 Hz. The tipper diagrams and induction arrows are shown in Figures 10 and 11. For reasons discussed later, the resistor is thought to be a pre-Hood intrusive complex, possibly consisting of Miocene dioritic rocks similar to the Laurel Hill-Still Creek complex exposed southwest of Government Camp.

On the basis of general model studies, we found that the amplitudes of the impedance functions (i.e., the apparent resistivity sounding curves and the related polar diagrams) are not a reliable indicator of conductive bodies at depth. One reason for this

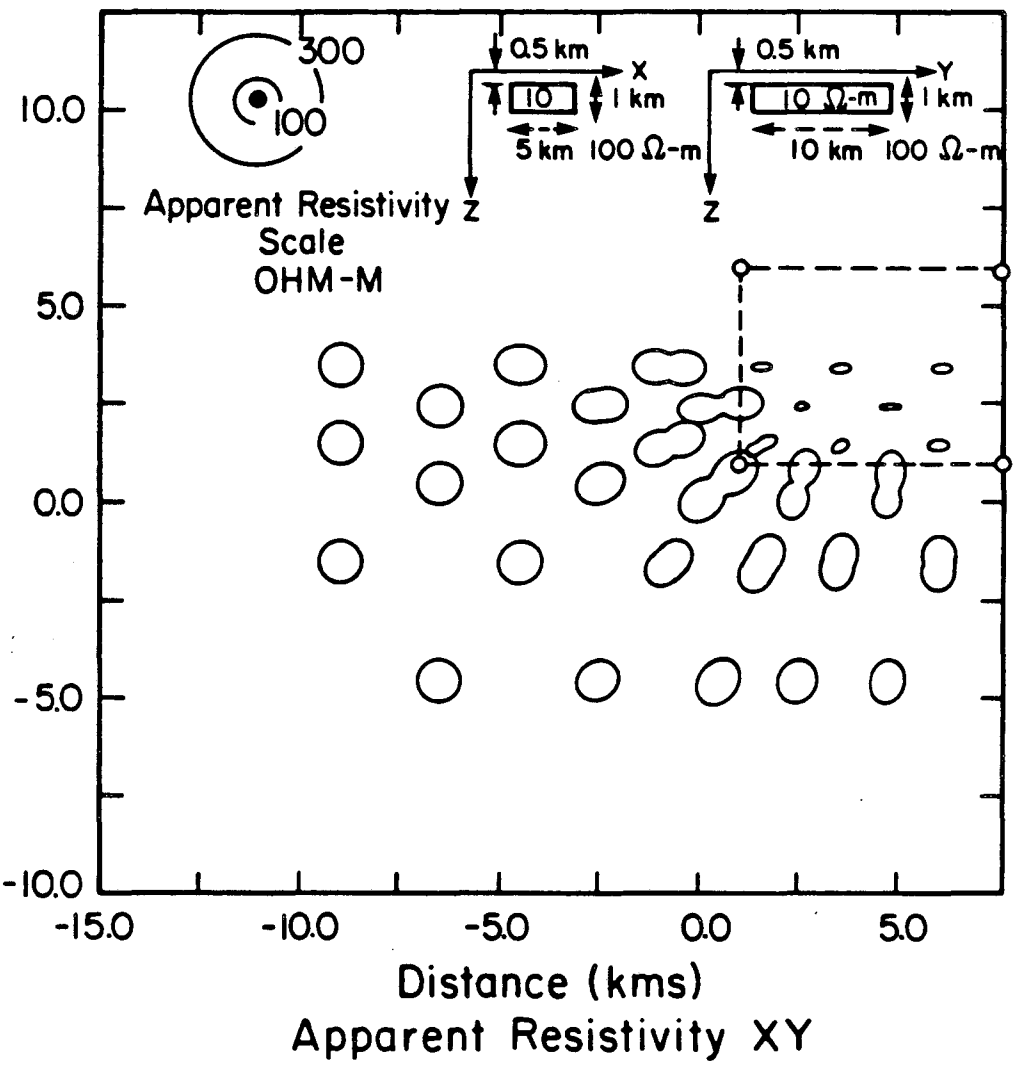

XBL 855-10493

Figure 7. Apparent resistivity polar diagrams at 0.01 Hz for the confined 3-D conductor shown in the insert diagram. Conductor horizontal dimensions are similar to those of the conductive region shown in Figure 6.

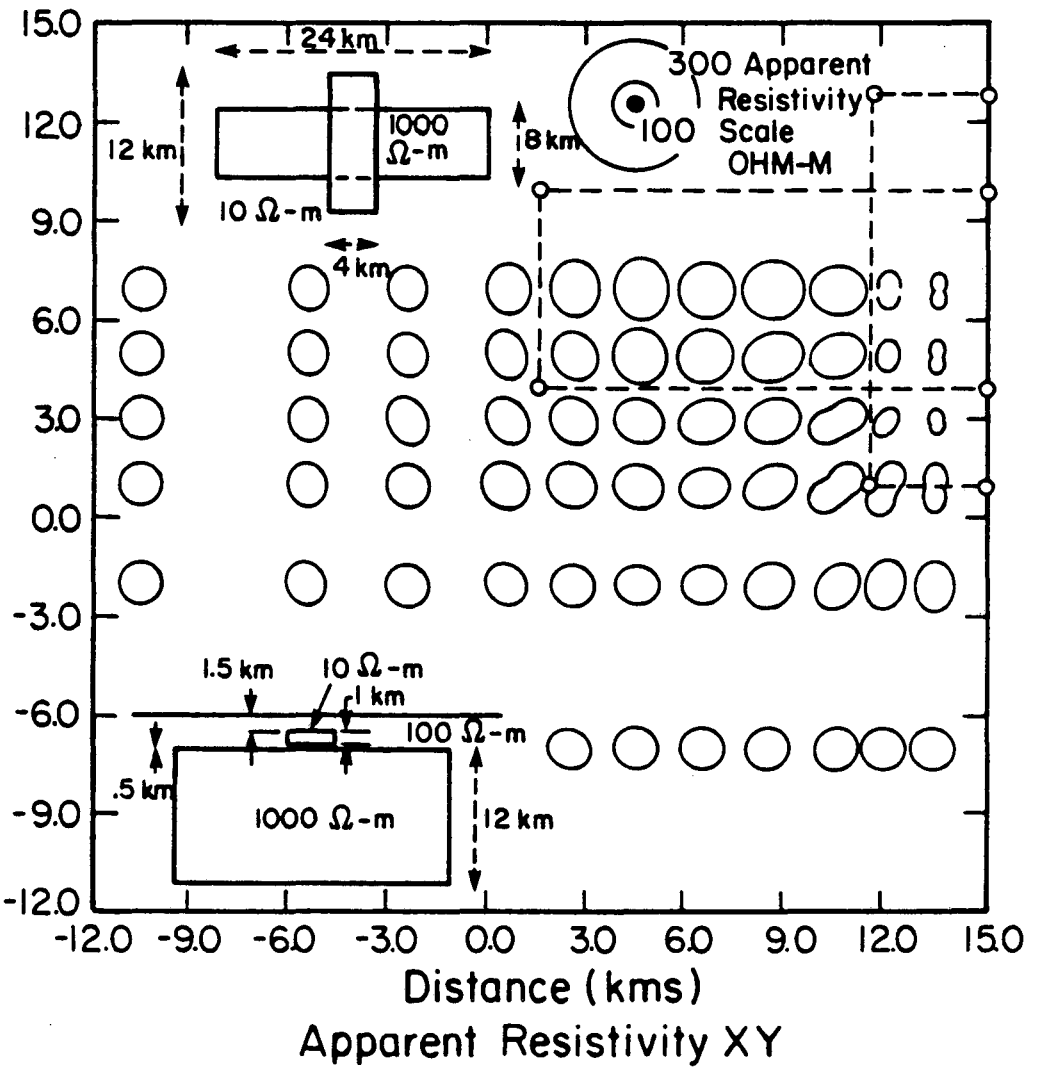

XBL 855-10494

Figure 8. Apparent resistivity polar diagrams for a two-body, 3-D model which consists of a shallow conductor, underlain by a resistive body of large depth extent. The model parameters are similar to those in Figure 7, except the frequency is 0.02 Hz.

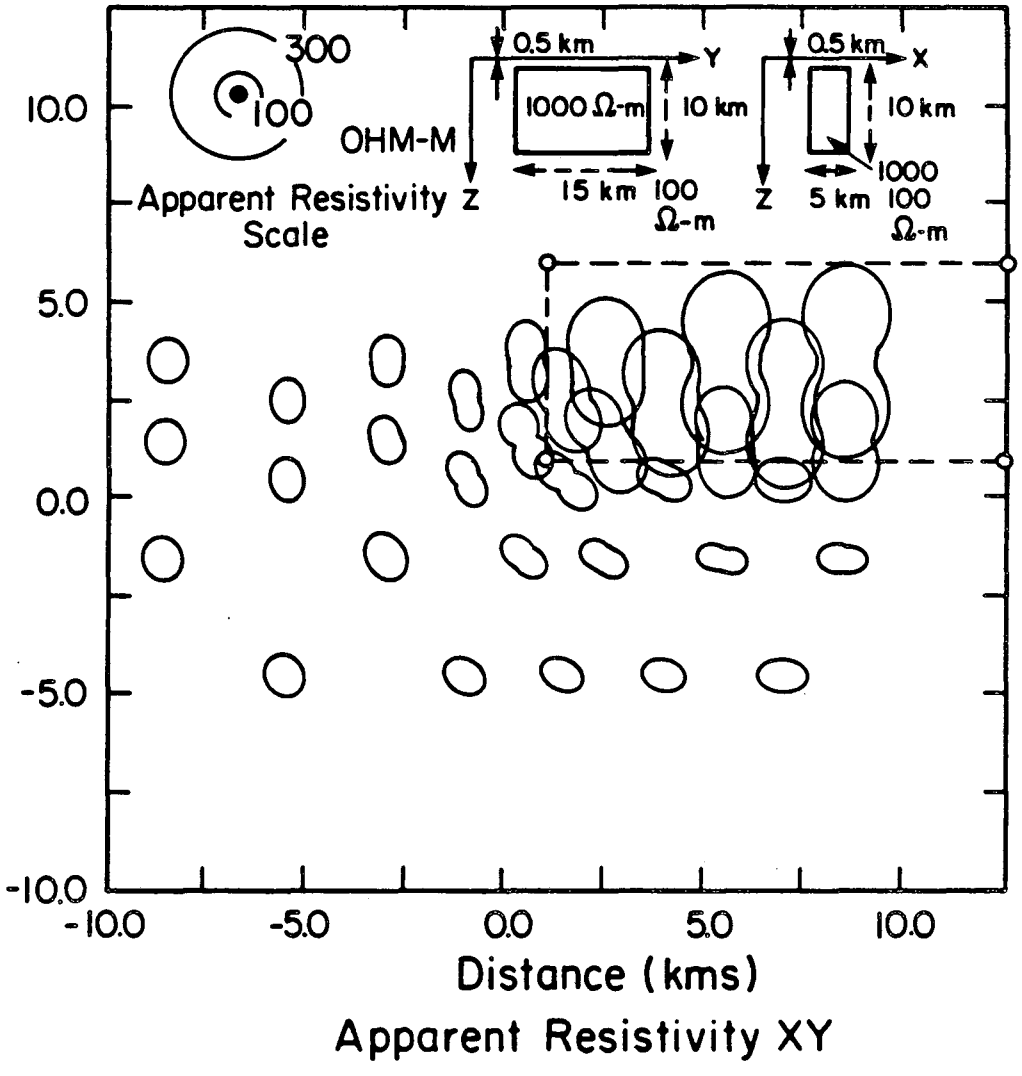

XBL 855-10491

Figure 9. Apparent resistivity polar diagrams calculated for the 3-D resistive body whose horizontal dimensions are similar to those of the lightly stippled area in Figure 6. The body parameters are specified in the insert. The frequency used in the calculation is 0.01 Hz.

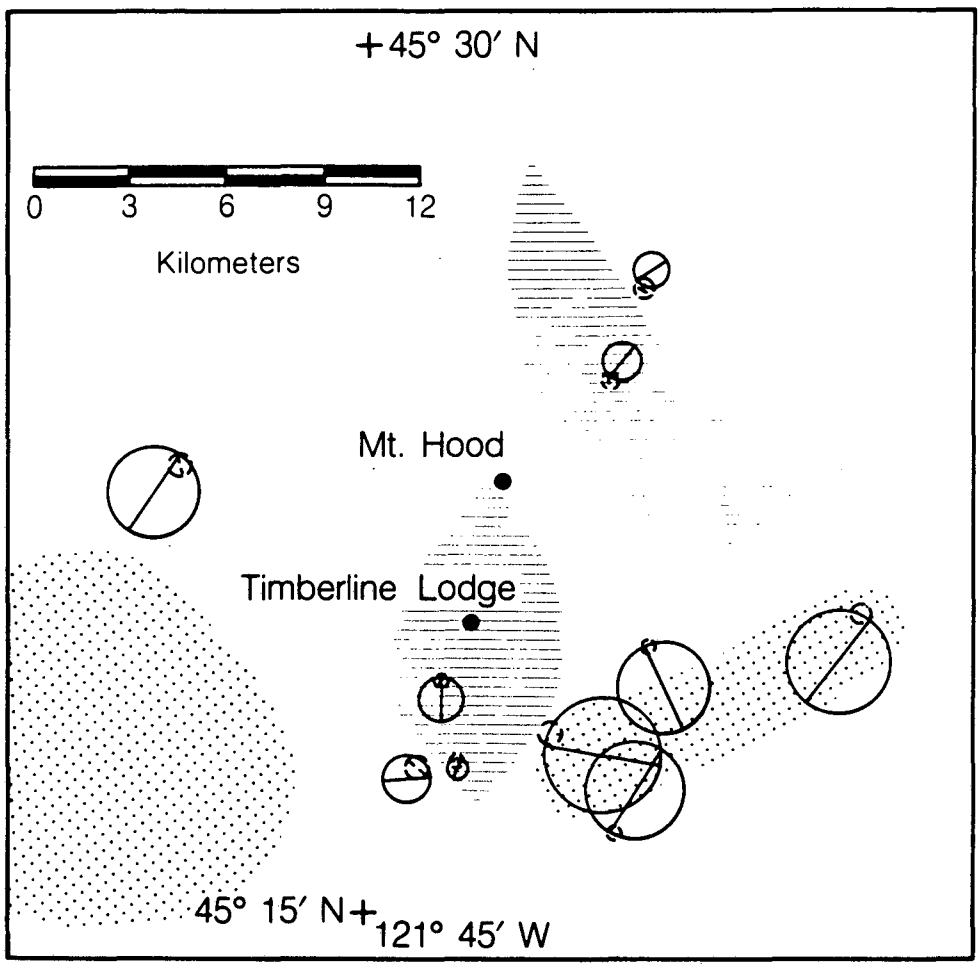

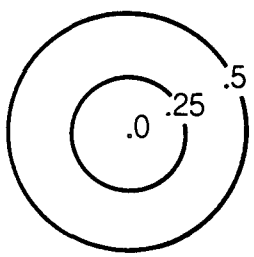

Induction Arrow Scale

XBL 864-10747

Figure 10. The complex tipper and induction arrows for the frequency band 1.0 to 5.0 Hz are shown. The larger circles with bisects represent the real components, while the smaller circles and their bisects represent the imaginary components. Stippled areas indicate the locations of near-surface resistive rock, the striped areas are locations of near-surface conductive rock.

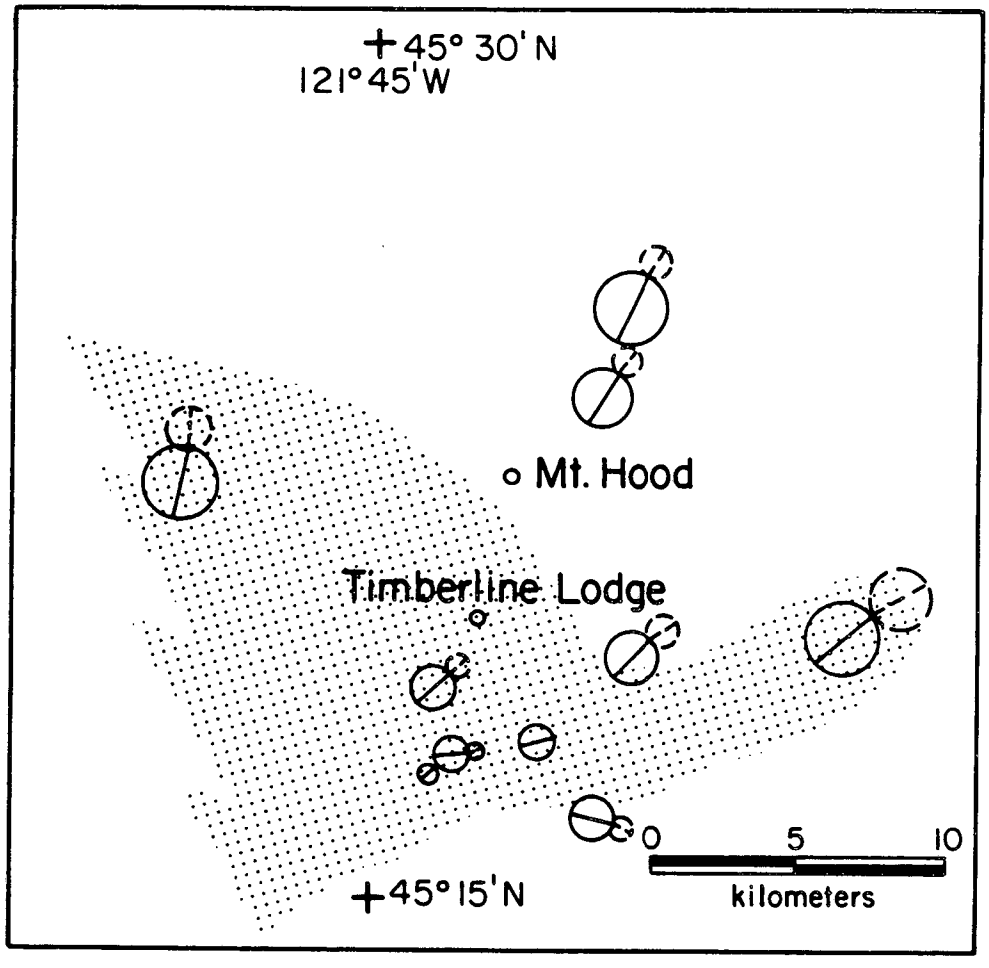

Figure 11. The complex tipper and induction arrows at the tensor MT stations for the 0.03 to 0.006 Hz bandwidth. Each dashed circle is the imaginary part of the geomagnetic transfer function (tipper) and the bisect is the imaginary part of the induction arrow. The solid circles and bisects are the real parts of the same complex field parameters. The stippled region is the approximate location of a resistive body at a depth of 4 to 6 km. The real components point toward, the imaginary components point away from, the more resistive body.

is that apparent resistivities are distorted over a broad band of frequencies by near-surface inhomogeneities. We therefore investigated various other measurement parameters to determine which one might be better for delineating a deep conductor. Numerical model calculations indicated that impedance phase with the primary electric field, E_y, aligned parallel to a 2-D or an elongate, 3-D deep conductor (in the so-called TE mode) was characterized by a minimum which provided a clear indication of the deep conductor (Fig. 12). Extensive 2-D sensitivity studies showed that a deep conductor causes a minimum in the phase spectrum at around 50 seconds period; the period of the peak is dependent on such parameters as depth, conductivity, and dimensions of the conductor. Moreover, the model studies showed that the 3-D conductor causes a band-limited anomaly in the phase spectrum, whereas the comparable 2-D conductor causes the distortion in the phase spectrum to extend to very long periods ($\sim$1000 s). To utilize this characteristic of the impedance phase, Mozley (1982) devised a phase-normalization procedure called "residual phase," which casts the phase information at a specific frequency or within a specified band into polar diagram form. The residual phase is defined as the absolute value of the impedance phase, calculated as a function of rotation angle, minus the minimum phase for all angles of rotation at each frequency. For these calculations, all phase values were shifted into the fourth quadrant (i.e., between -90 and 0°). The resulting figure-eight diagrams are extremely sensitive to conductor strike. The maximum residual phase is parallel to strike (Fig. 13) and the direction is less distorted by surface conductivity variations than are the apparent resistivities. An example of the residual phase polar diagrams for the model introduced in Figure 12 is shown in Figure 13. Note that the polar diagrams in the vicinity of the conductor are elongated parallel to the strike of the conductor at the frequency of the local minima in the impedance phase spectra.

The relationship between residual phase and a deep conductor is illustrated in the example of data at cluster 1, which, like data at clusters 2 and 7, were relatively

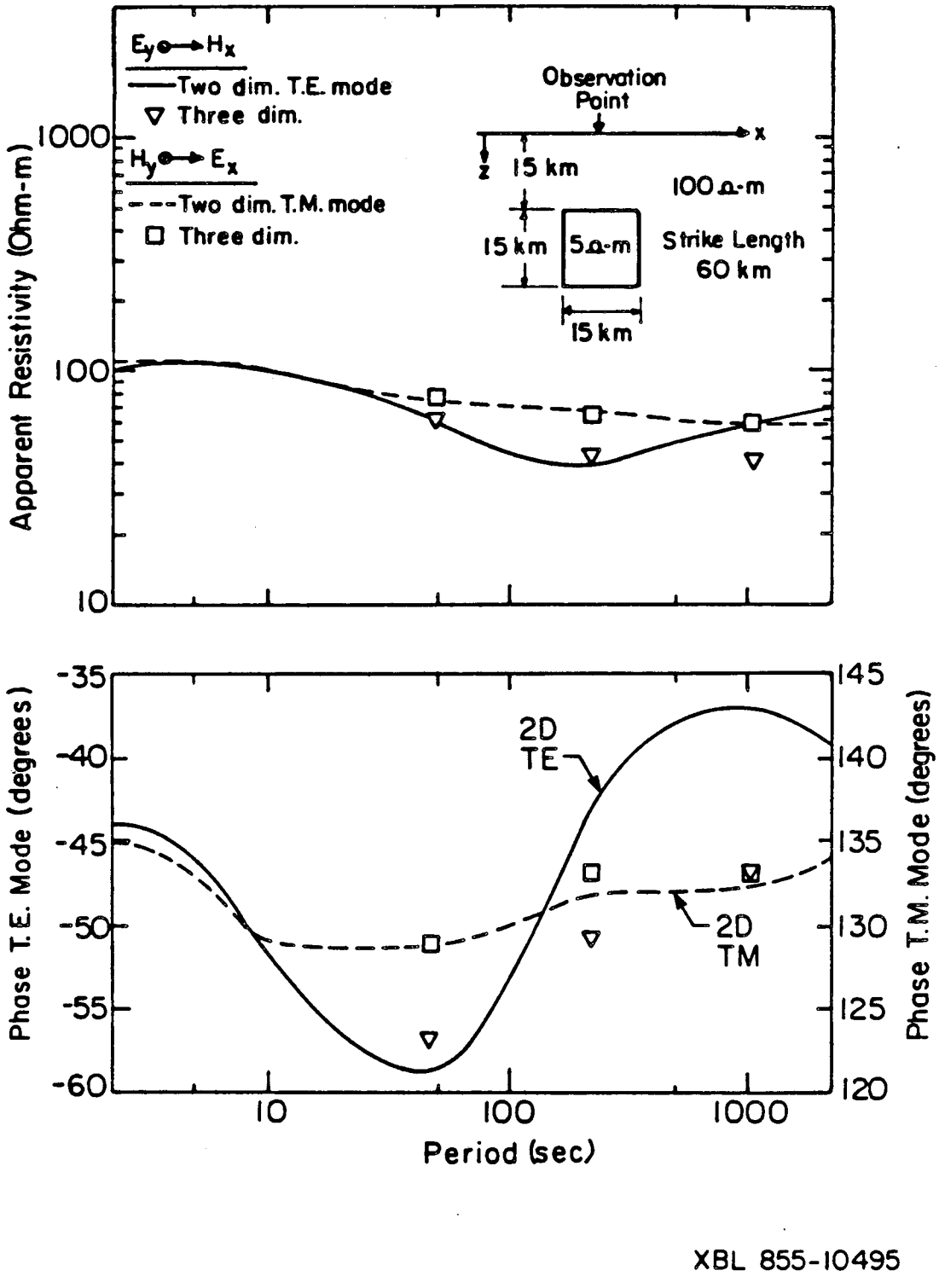

Figure 12. The calculated amplitude and phase spectra for a point of observation directly over an elongate conductor at a depth of 15 km. The symbols indicate the responses for a 3-D conductor of strike length of 60 km. The solid and broken curves are the responses for the 2-D conductor of infinite strike length.

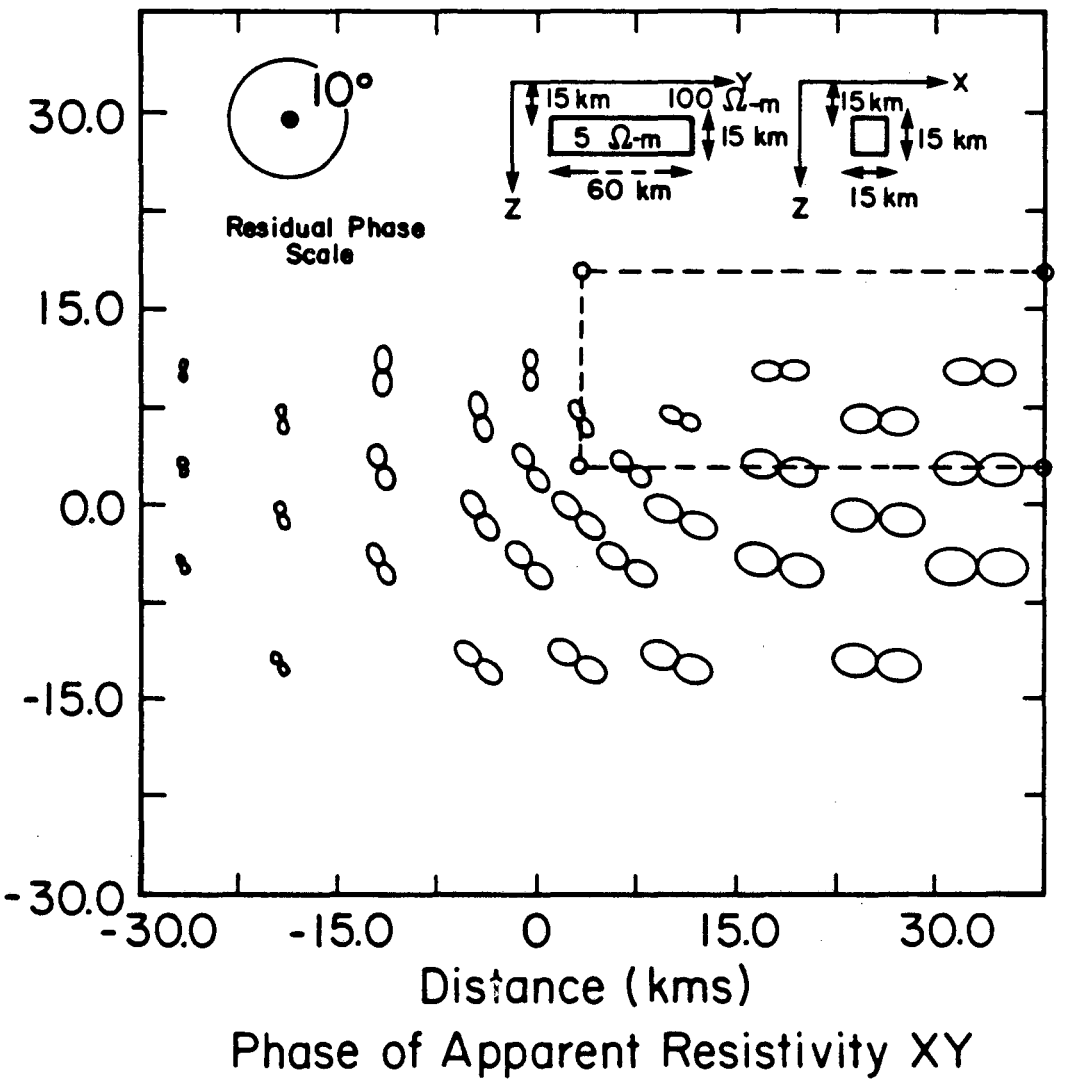

XBL 855-10490

Figure 13. Residual phase polar diagrams for the elongate 3-D deep conductor shown in Figure 12 at the frequency of 0.02 Hz. The observation positions are limited to one quadrant, as the model has two planes of symmetry.

undistorted by near-surface inhomogeneities. A set of smoothed polar diagrams was calculated for each of the five numbered frequency bands (Fig. 14). The bands were selected to focus attention on specific frequency characteristics observed in both the impedance and tipper estimates throughout the survey area. The most important characteristic is the local minimum in the impedance phase in band 4. The dominant frequency characteristic observed in the tipper responses were the 0° and $\pm 180^\circ$ phase values located in band 1 and between bands 3 and 4. The impedance parameters for station 1 were rotated into the principal direction at each frequency by maximizing the off-diagonal terms of the impedance tensor, as described by Vozoff (1972). The impedance phase characteristics were interpreted through model studies to indicate an elongate conductor at 10 to 15 km beneath the area. The phase maximum of about -50° occurs near a period of 75 s in the Z_{xy} impedance element (band 4). At this station the absolute minimum phase is associated with the impedance element Z_{yx} and has a value of about -38°. The phase difference of 12° is the residual phase, and in this case the direction giving the maximum value for the residual phase was the same as the principal direction found from maximizing the off-diagonal elements of the impedance tensor. These directions would not be the same, in general, if local, near-surface inhomogeneities were present.

The residual phase polar diagrams for all the band 4 field data are shown in Figure 15. These diagrams have a surprising amount of spatial consistency and indicate a conductive body at depth with a strike of approximately N10°W. The shaded region gives the approximate position of the deep conductor, which looks like a 2-D body under the volcano. The lightly stippled area in the figure is the near-surface resistor as determined from apparent resistivities and induction arrows. The distortions in the phase diagrams are probably due to multibody 3-D effects, but those were not modeled.

For the 2-D modeling we selected a line of section, indicated by the straight line in Figure 6, that is orthogonal to the strike of the regional conductor. The absence of

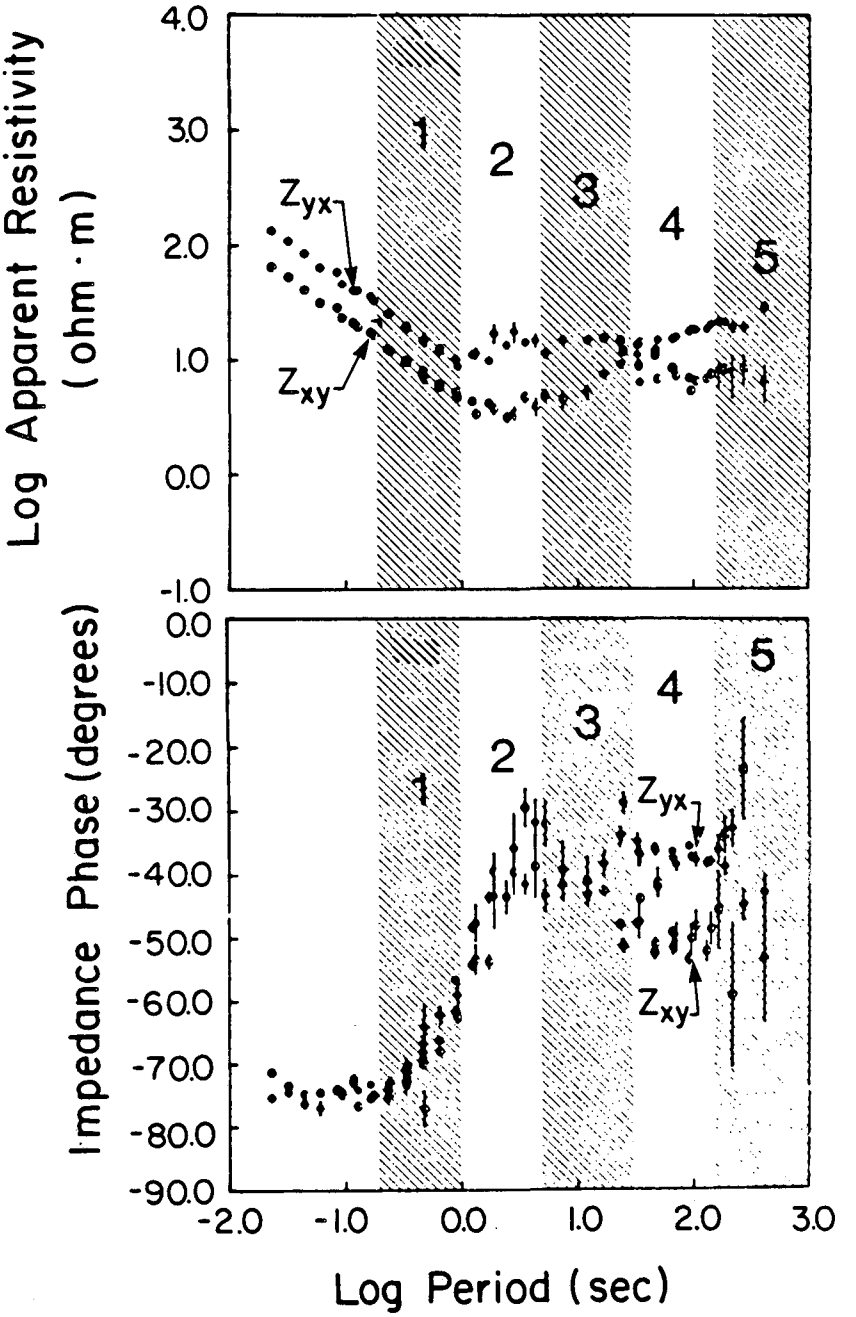

Figure 14. An example of the apparent resistivities and impedance phases at station 1, where there was only moderate distortion due to near-surface inhomogeneities. The five bands show the bandwidths over which field data were averaged to generate five sets of polar diagrams.

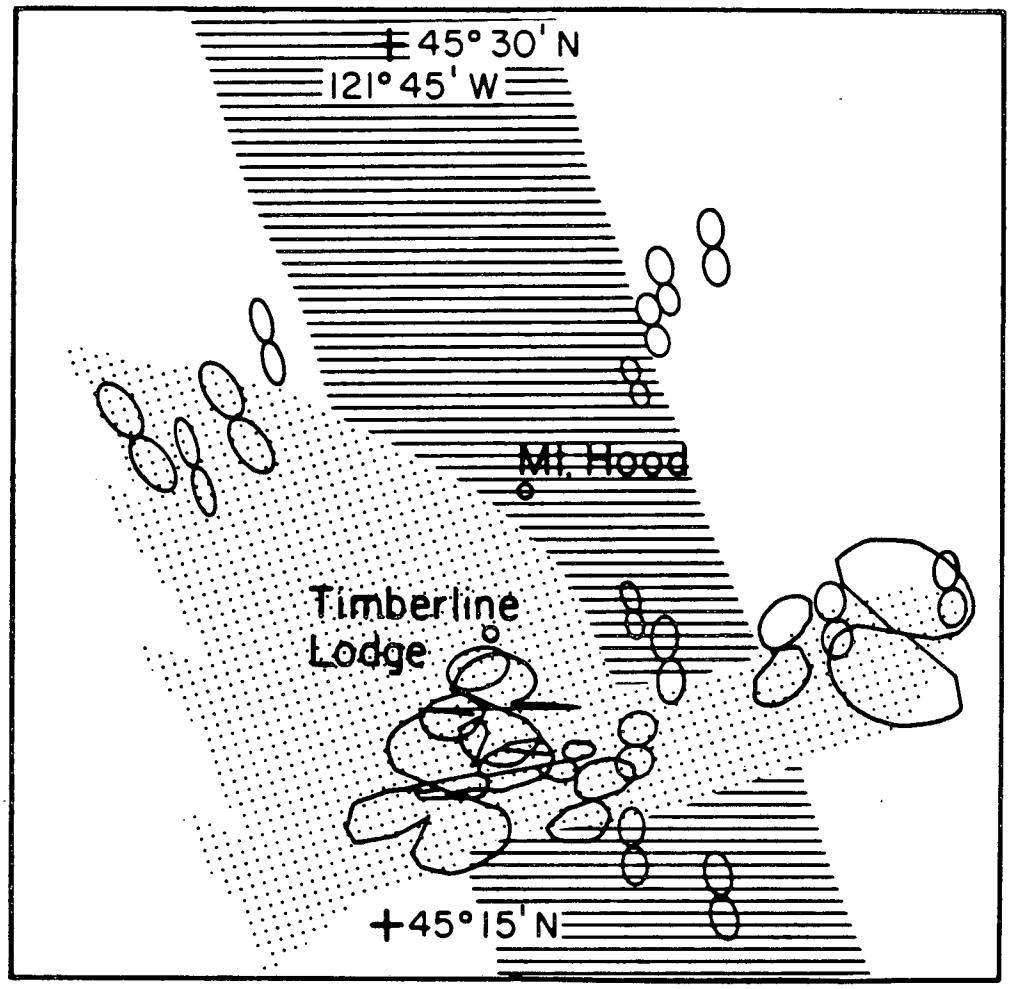

Figure 15. Residual phase polar diagrams for field data in band 4 (0.03 to 0.006 Hz). The inferred deep conductor is indicated by the region with banded shading. The shallower resistive region, from Figure 11, is indicated by the stippled pattern.

surface inhomogeneities and the consistent principal directions found from the residual phase analysis suggested that a reasonable estimate for the conductivity variations in the area could be found by projecting apparent resisitivity and phase data onto this section and then applying a 2-D parameterization to simulate the observed data set. The results of the inversion are shown in Figure 16. Two major constraints were applied to the 2-D model. We placed a deep conductor (1 ohm·m) at 12 km depth, and we used the resistivity logs from wells OMF-7A and OMF-1, drilled to depths of 1836 and 1220 m, respectively, to fix the shallow resistivities (Blackwell et al., 1982). The subvolcanic conductor, 3 ohm·m near the center of the model, does not significantly affect the calculated impedance functions; it can be left out without greatly affecting the fit between calculated and observed values. Besides being consistent with a geologic concept of a hot and fractured central conduit, the conductor location was suggested by an interpretation of the induction arrow and complex tipper parameters applied to 2-D and 3-D bodies (Mozley, 1982).

Before we discuss the geologic significance of the electrical model, it would be appropriate to comment on the fit between calculated 2-D and observed values, as illustrated in Figures 17 and 18. Fits to both TE and TM data at stations on both ends of the profile are similar in quality; the symbols are field data, the solid and broken lines are calculated. At low frequencies the match is not good for the phase of the TE mode. This would indicate that the deep, 1-ohm·m conductor has a finite strike length. However, the low-frequency mismatch can also be resolved by providing the appropriate conductivity distribution at depths below 50 km. For example, a deep conductor in the mantle would radically reduce the phase response of the TE mode at low frequencies and thereby improve the fit. Because of limited spatial sampling, we cannot tell which of the above models is the more appropriate.

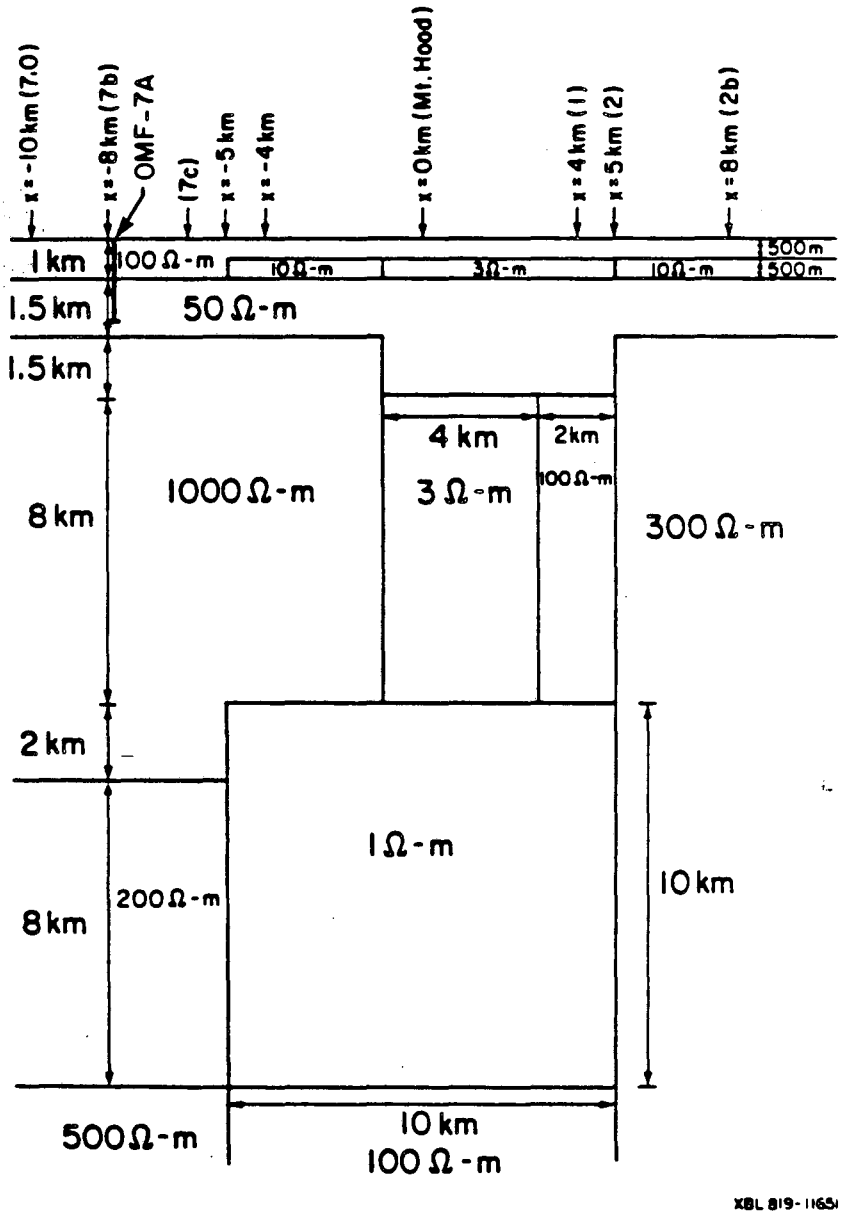

Figure 16. The 2-D resistivity distribution for the profile shown in Figure 6.

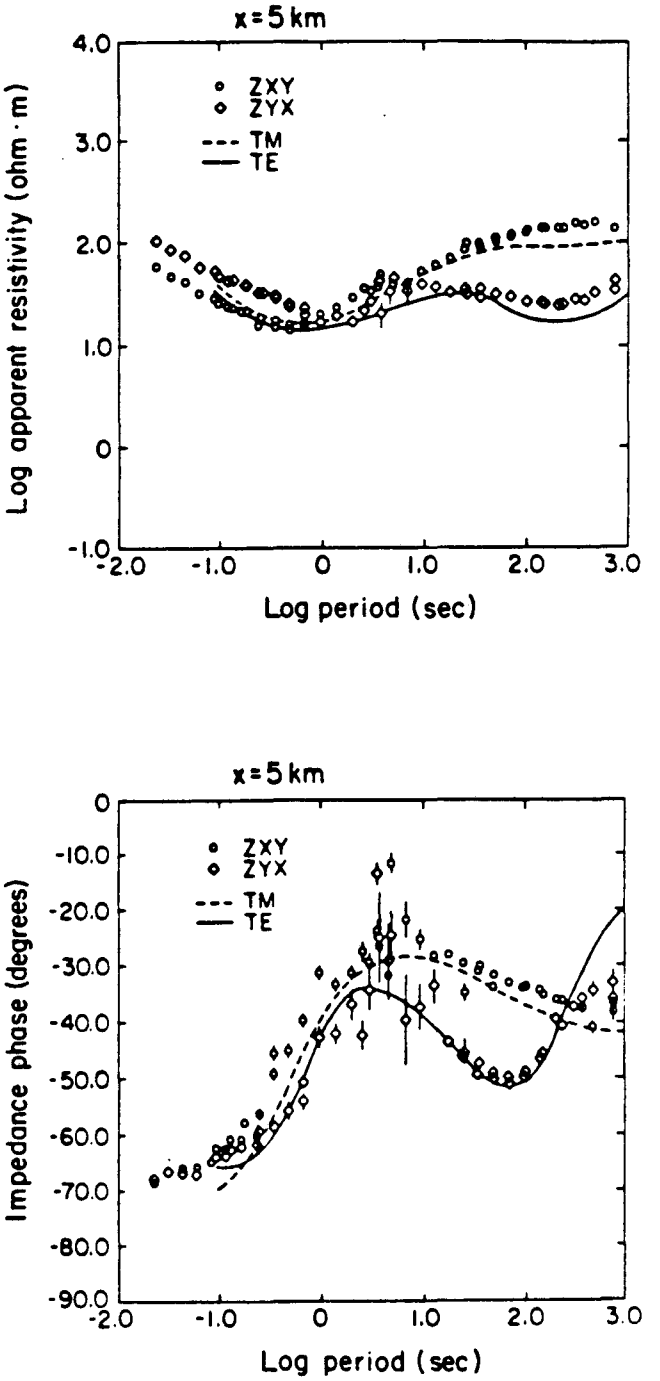

Figure 17. A comparison of the calculated parameters for the 2-D model of Figure 16 (solid and broken curves) and the actual field data at station 2 (x = 5 km).

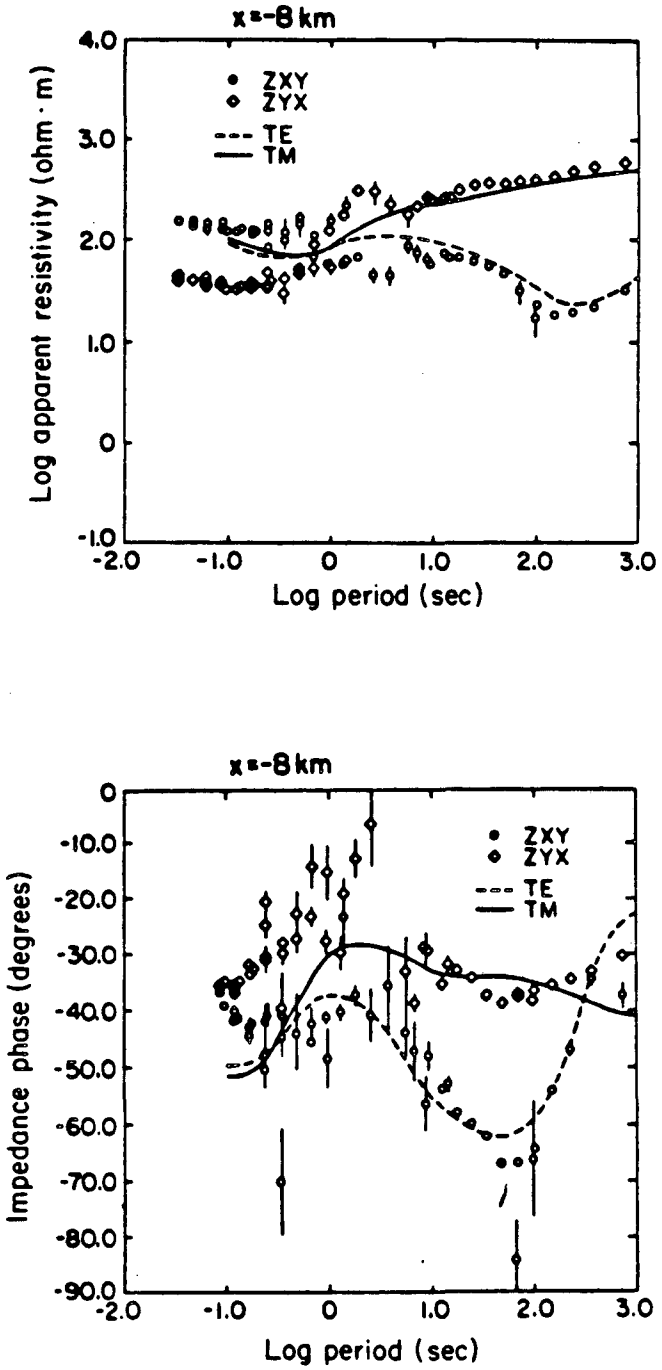

Figure 18. Another comparison, similar to that shown in Figure 17, but for the MT sounding station 7B, located on the southwestern end of the profile. Notice that the fits to the low frequency Z_{xy} phase data are poor, suggesting either that the deep conductor has a finite strike length or that an even deeper conductor is present.

DISCUSSION OF THE ELECTRICAL MODEL

Although the use of 1-, 2-, and 3-D analyses of the MT data did not yield a complete and totally satisfying electrical model for the region, discrete anomalous areas were identified. Using a little subjective license, these were assembled into a general composite model (Fig. 19) The features shown are biased to some extent by the locations of the sounding points. Shallow conductors (I and II) probably represent saturated and relatively permeable pyroclastics at depths of about 500 m. Hydrogeologically, these conductors may be related to zones of meteoric waters (mainly snowmelt) heated to 150-200 ° C by hot rocks at the summit, the waters cooling as they flow laterally away from the apex (Wollenberg et al., 1979). The computed depths were determined from the 1-D MT inversions and are supported by controlled-source electromagnetic soundings (Goldstein et al., 1982). The lateral boundaries of the shallow conductors, where indicated, were determined on the basis of the 2-D and 3-D modeling, using the tippers and induction arrows in the bandwidth 1 to 5 Hz.

The elongate, 1000-ohm·m resistor on the southeast side of the cone (III) was identified from a 3-D analysis of apparent resistivity and induction arrows. The feature may represent a concealed and resistive igneous stock, evidenced by a prominent group of quartz diorite dikes in the White River area (Keith et al., 1985).

There also seems to be a broad area of resistive rocks (IV) beneath the western flank of the volcano. The general boundaries of this zone were determined from distortions in the impedance parameters and from the 2-D analysis. On the basis of lithologies from hole OMF-7A (Priest et al., 1982), the resistor consists of a thick section of Columbia River basalts and underlying Eocene (?) greenstones cut by thick dikes or sills of Pliocene microquartz diorite. Well logs show that the depth to these higher-density, lower-porosity, more-resistive rocks is about 800 m, which is the depth to the top of the Columbia River basalts. The electrical resistor is also consistent with the high seismic velocities found from a large-scale refraction survey (Kohler et al., 1982). Figure 20

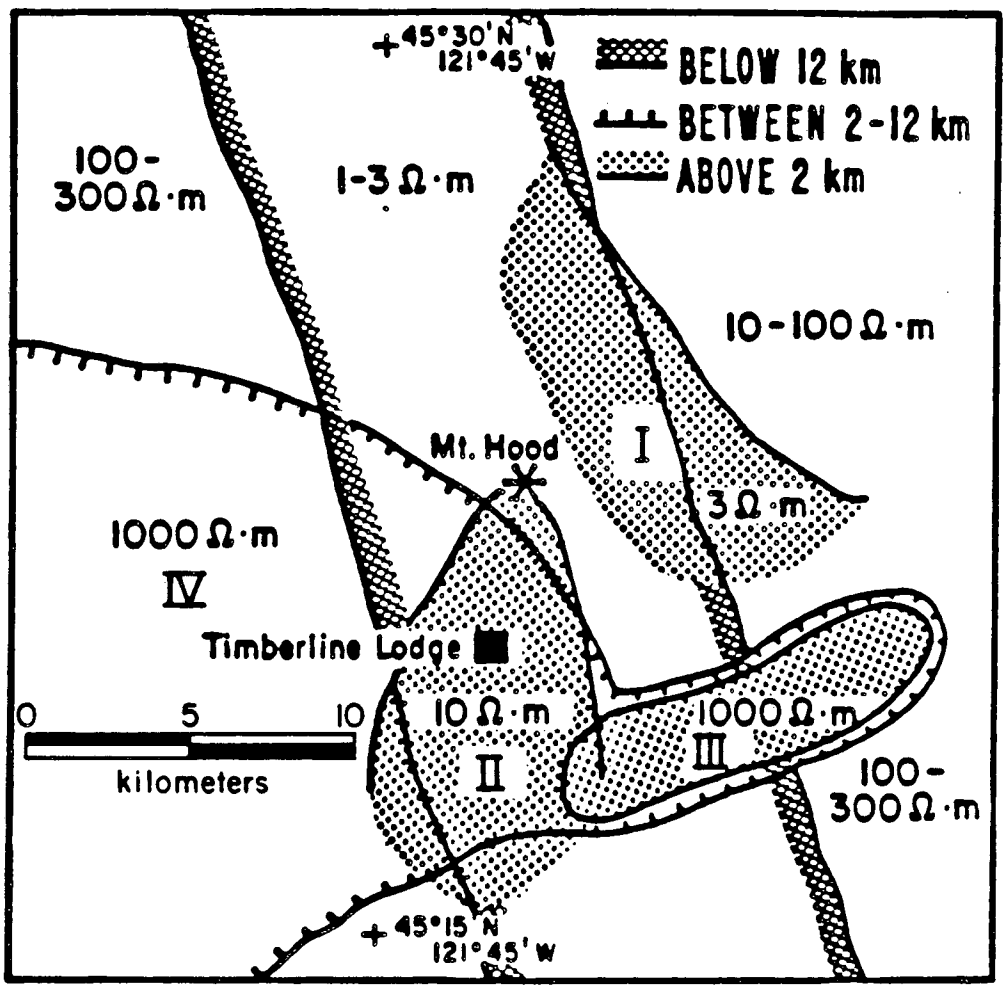

XBL 855-10483

Figure 19. A composite model of the resistivity distribution around Mount Hood.

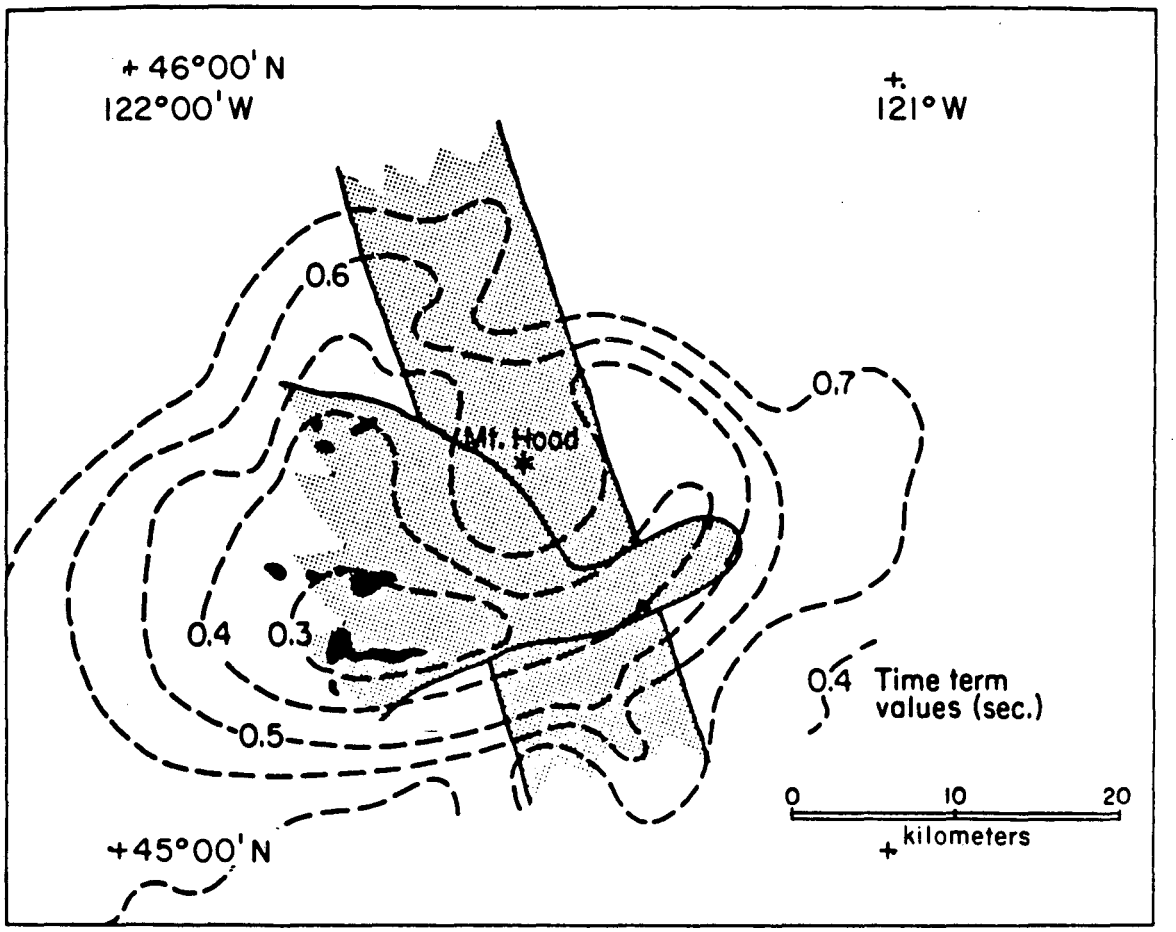

XBL 855-10484

Figure 20. Components of the resistivity model (Fig. 19) superimposed on the time-term results of Kohler et al. (1982) for source-receiver separations of 19.7 to 40 km. The broken contours are the time-term values in seconds; they outline a high-velocity zone that seems to agree with the resistive region. The small black areas are the outcropping Pliocene quartz-diorite intrusives and later andesite plugs indicated by Wise (1969).

shows the good concordance between the high velocity (expressed by the low values of the time-term results), the outline of the resistive region, and the outcropping Pliocene plugs and cupolas (Wise, 1969). There is also a weak correlation of these features and the Bouguer gravity (Fig. 21) (Couch et al., 1981).

The last and deepest feature in Figure 19 is the elongate, approximately 2-D conductor at a depth of 12 km. Its strike direction was clearly indicated from the impedance phase, and its depth, width, and resistivity were determined from the 2-D modeling. The conductor may have a depth extent of 10 km. Mozley (1982) argued that the conductor could indicate a partial silicic melt on the basis of terrain-corrected temperature gradients of 60 to 70 °C/km that were measured in holes around the volcano (Steele et al., 1982). It is perplexing, however, that a partial melt zone with physical dimensions as large as those indicated has not produced a measurable P-wave velocity anomaly. The absence of a P-wave delay anomaly beneath Mount Hood (Weaver et al., 1982) and beneath other High Cascade stratovolcanoes has been attributed to the possible small size of these melt zones ($<$ 5 km in diameter, the nominal resolution of inversion techniques) and to the very complex vertical and lateral variations in near-surface velocities (Iyer et al., 1982). It is also difficult to envision geologically so large a volume of partial melt in the context of the rates and volumes of High Cascade volcanism near Mount Hood during the last 0.1 Ma. We therefore propose that the conductor could be caused by a brine-filled microfractured crust in which there may be small zones of partial melt. In support of the microfracture hypothesis, it should be noted that the High Cascades have been undergoing east-west extension for at least the last 16 Ma, as evidenced by the alignment of cinder cones and widely spaced stratovolcanoes, the trend of normal faults that bound the High Cascades graben (Couch et al., 1982), and the direction of faults, fractures, and the presence of basaltic dikes near Mount Hood in the Columbia River Basalt Group lavas (Beeson and Moran, 1979).

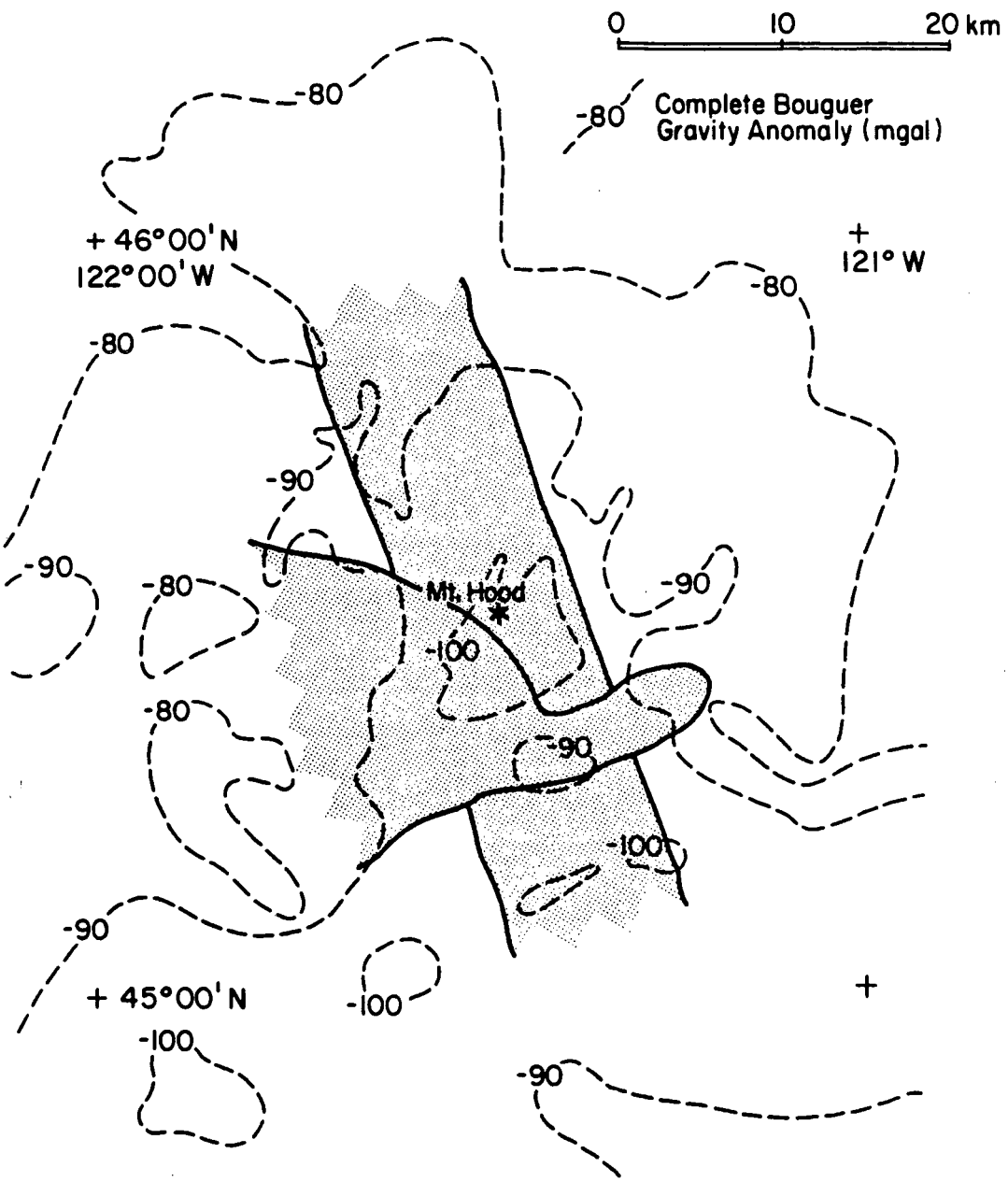

Figure 21. Components of the resistivity model (Fig. 19) superimposed on the Bouguer gravity map of Couch et al. (1981).

The 2-D cross section (Fig. 16), running perpendicular to the strike of the deep conductor, deserves a few additional words of discussion. Although we placed few geologic constraints on the 2-D interpretation, features in the resulting electrical model are in rather good general agreement a general schema proposed by Henley and Ellis (1983) for a hypothetical geothermal-hydrothermal system associated with an active island-arc composite andesite volcano (Fig. 22). The only verified hydrothermal system at Mount Hood occurs in the summit-crater area, where meteoric water (snowmelt) is heated by hot rocks to produce boiling point fumaroles and waters that move laterally away from the summit in shallow, permeable pyroclastics or brecciated flows (Wollenberg et al., 1979; Sorey, pers. comm., 1985). From a study of drilling results on the flanks of Mount Hood, Steele et al. (1982) find no evidence for vertical permeability in the surficial volcanics. Whether there exists a larger, deeper hydrothermal zone at temperatures of 300 °C adjacent to the central conduit has not yet been indicated by geophysics or tested by drilling.

CONCLUSIONS

The question of whether a partial melt zone exists beneath the axis of the High Cascades may not have been answered unequivocally by the MT results around Mount Hood, even though the data show evidence for an elongate conductor striking N10 °W and extending from a depth of 12 km down to 22 km. Although the local and regional temperature gradients indicate a silicic melt could occur at depths of 12 km, other factors such as the absence of a teleseismic P-wave anomaly, the enormous volume of the conductor relative to the volume and rates of volcanism in the last 0.1 Ma and the east-west extensional stresses that have existed for the last 16 Ma suggest that the conductor may be due mainly to brine-filled microfractures.

That the deep conductor was resolved at all by MT is something of a surprise in view of the limited spatial and frequency window available. This, however, is not the

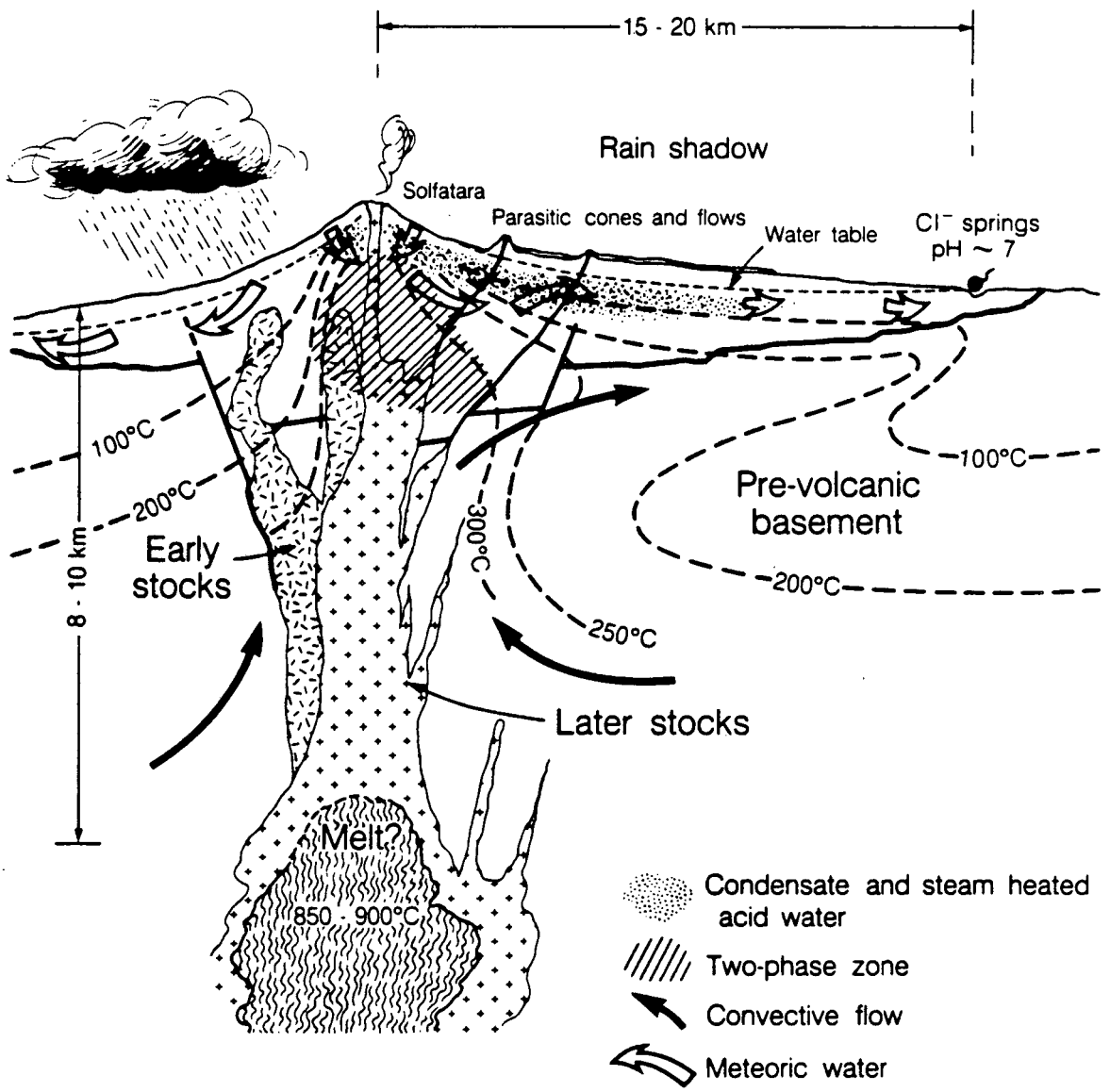

Figure 22. Conceptual geologic-hydrologic model for an andesitic stratocone. Snowmelt is heated to boiling by hot rocks in the central conduit; condensate and other heated waters flow outward in permeable volcanic strata or guided by a fracture system. These waters are diluted by cold meteoric water and may emerge as cold near-neutral springs at some distance from summit. A deep circulating hydrothermal system may exist in fractured rocks beneath the summit and a small partial melt zone may remain at depths of 8-10 km.

only conductor encountered. A shallow conductor at a depth of around 0.5 km may be a flow of warm water away from the summit in permeable volcanics. A conductor at an intermediate depth of about 5 km could be related to the fractured subvolcanic conduit, but there is not compelling evidence for this conductor. Finally, there is evidence for a very deep conductor that might be a melt zone in the upper mantle. The relatively narrow spatial and frequency window through which we probed the crust allows for many ambiguities, a common problem of geophysical interpretations.

The validity of our crustal model can be tested by the acquisition and interpretation of detailed MT data collected at other accessible and geologically interesting places across the High Cascades. On the basis of the experience reported here, it seems necessary to collect data at some stations to frequencies as low as 0.001 Hz. We would also strongly recommend tight clusters of stations, with individual stations 2 to 5 km apart. This procedure is necessary to identify and understand the effects of near-surface inhomogeneities on the sounding data.

Because it is highly likely that impedance amplitudes will be distorted at some stations by local surface conductivity variations, the detection of deep conductors may depend on the proper analysis of impedance phase characteristics. Whereas surface inhomogeneities cause broadband effects on impedance amplitude and dominate the tipper responses, they affect phase only at high frequencies. The location and strike direction of a deep conductor becomes possible to define in the presence of near-surface inhomogeneities when the impedances are rotated into the principal conductivity directions indicated by the residual phase diagrams for the frequency band giving a local minimum in the impedance phase.

ACKNOWLEDGEMENTS

This work was supported by the Assistant Secretary for Conservation and Renewable Energy, Office of Renewable Technology, Division of Geothermal and Hydropower Technologies of the U.S. Department of Energy under Contract No. DE-AC03-76SF00098. The data acquisition and processing were successfully completed through the efforts of several individuals, to whom we are most grateful. Ramsey Haught played a major factor in data acquisition. Victor Labson, Thomas Gamble, and Wolfgang Goubau assisted in the processing phase of the study. Gary Oppliger, Keeva Vozoff, and Ki Ha Lee helped with the modification of 2-D and 3-D numerical codes. Francis Bostick provided advice on data interpretation. Terry Keith and George Priest offered extremely helpful geological information.

References

Allen, J.E., The Cascade Range volcano-tectonic depression in Oregon, *Trans. Lunar Geol. Field Conf.*, 21-23, 1966.

Atwater, T., Implications of plate tectonics for the Cenozoic tectonic evolution of western North America, *Geol. Soc. Am. Bull., 81* (12), 3513-3535, 1970.

Bacon, C.R., Geology and geophysics of the Cascade Range (abstr.), paper presented at 51st Annual International Meeting, Soc. Expl. Geophys., Los Angeles, Calif., Oct. 11-15, 1981.

Beeson, M.H., and M.R. Moran, Stratigraphy and structure of the Columbia River Basalt Group in the Cascade Range, Oregon, *in* Geothermal Resource Assessment of Mount Hood, Oregon Dep. Geol. Miner. Ind., *Final Rep. RLO-1040,* 5-77, 1979.

Black, G.L., Heat flow in the Oregon Cascades, *in* Priest, G.R., and Vogt, B.F., eds., Geology and Geothermal Resources of the Central Oregon Cascade Range, Oregon Dep. Geol. Miner. Ind., *Spec. Pap. 15,* 69-76, 1983.

Blackwell, D.D., Heat flow and energy loss in the western United States, *Geol. Soc. Am. Memoir 152,* 175-208, 1978.

Blackwell, D.D., D.A. Hull, R.G. Bowen, and J.L. Steele, Heat flow of Oregon, Oreg. Dep. Geol. Miner. Ind., *Spec. Pap. 4,* 42 pp., 1978.

Blackwell, D.D., C.F. Murphy, and J.L. Steele, Heat flow and geophysical log analysis for OMF-7A geothermal test well, *in* Priest, G.R., and Vogt, B.F., eds., Geology and Geothermal Resources of the Mount Hood Area, Oregon Dep. Geol. Miner. Ind., *Spec. Pap. 14,* 47-56, 1982.

Callaghan, E., Some features of the volcanic sequence in the Cascade Range in Oregon, *Trans., Am. Geophys. Union,* 243-249, 1933.

Carey, S., and H. Sigurdsson, The May 18, 1980 eruption of Mount St. Helens, 2. Modeling of dynamics of the Plinian phase, *J. Geophys. Res., 90* (B4), 2948-2958, 1985.

Couch, R.W., and M. Gemperle, Gravity measurements in the area of Mount Hood, Oregon, *in* Geothermal Resource Assessment of Mount Hood, Oreg. Dep. Geol. Miner. Ind., *Open File Rep. 0-79-8,* 137-189, 1979.

Couch, R.W., G.S. Pitts, D.E. Braman, and M. Gemperle, Free-air gravity anomaly map and complete Bouguer gravity anomaly map, Cascade Mountain Range, Northern Oregon, Oreg. Dep. Geol. Miner. Ind., *Geol. Map Ser., GMS-15,* 1981.

Couch, R.W., G.S. Pitts, M. Gemperle, D.E. Braman, and C.A. Vene, Gravity anomalies in the Cascade Range, Oregon: Structural and thermal implications, Oreg. Dep. Geol. Miner. Ind., *Open File Rept. 0-82-9,* 1982.

Crandall, D.R., Recent eruptive history of Mount Hood, Oregon, and potential hazards from future eruptions, *U.S. Geol. Survey Bull. 1492,* 81 pp., 1980.

Davis, G.A., Late Cenozoic tectonics of the Pacific Northwest with special reference to the Columbia Plateau, Washington Power Supply System Final Safety Analysis Report, *Appendix 2.5N,* 44 pp., 1981.

Flanagan, G.F., and D.L. Williams, A magnetic investigation of Mount Hood, Oregon, *J. Geophys. Res., 87* (B4), 2804-2814, 1982.

Gamble, T.D., W.M. Goubau, and J. Clarke, Magnetotellurics with a remote magnetic reference, *Geophysics, 44* (1), 53-68, 1979.

Goldstein, N.E., E. Mozley, and M. Wilt, Interpretation of shallow electrical features from electromagnetic and magnetotelluric surveys at Mount Hood, Oregon, *J. Geophys. Res., 87* (B4), 2815-2828, 1982.

Henley, R.W., and A.J. Ellis, Geothermal systems ancient and modern, a geochemical review, *Earth Sci. Rev., 19,* 1-50, 1983.

Hermance, J.F., and R.E. Thayer, The telluric-magnetotelluric method, *Geophysics, 40,* 664-668, 1976.

Hildreth, W., Gradients in silicic magma chambers: Implications for lithospheric magmatism, *J. Geophys. Res., 86* (B11), 10153-10192, 1981.

Iyer, H.M., A. Rite, and S.M. Green, Search for geothermal heat sources in the Oregon Cascades by means of teleseismic P-residual technique (exten. abstr.), presented at 52nd Annual International Meeting, Soc. Expl. Geophys., Dallas Texas, Oct. 17-21, 1982.

Jupp, D.L.B., and K. Vozoff, Stable iterative methods for the inversion of geophysical data, *Geophys. J.R. Astro. Soc., 42,* 957-976, 1975.

Keith, T.E.C., J.M. Donnelly-Nolan, J.L. Markman, and M.H. Beeson, K-Ar ages of rocks in the Mount Hood area, Oregon, *Isochron West, 42,* 12-16, April, 1985.

Kohler, W.M., J.H. Healy, and S.S. Wegener, Upper crustal structure of the Mount Hood, Oregon, region as revealed by time term analysis, *J. Geophys. Res., 87* (B1), 339-355, 1982.

Law, L.K., D.R. Auld, and J.R. Booker, A geomagnetic variation anomaly coincident with the Cascade volcanic belt, *J. Geophys. Res., 85,* 5297-5302, 1980.

Lee, K.H., D.F. Pridmore, and H.F. Morrison, A hybrid three-dimensional electromagnetic modeling scheme, *Geophysics, 46* (5), 796-805, 1981.

Mozley, E.C., An investigation of the conductivity distribution in the vicinity of a Cascade volcano: Ph.D. Thesis, Univ. of Calif., Berkeley, Lawrence Berkeley Laboratory *Rept. LBL-15671,* 386 p., 1982.

Pridmore, D.F., Three-dimensional modeling of electric and electromagnetic data using the finite element method: Ph.D. Dissertation, Univ. of Utah, 1978.

Priest, G.R., N.M. Woller, and S. Evans, Late Cenozoic modification of calc-alkalic volcanism, central Oregon Cascades (abstr.): Am. Acad. Advancement of Sci. Abstr. with Prog., 1981 Pacific Division Meeting, p. 32, 1981.

Priest, G.R., Overview of the geology and geothermal resources of the Mount Hood area, Oregon: *in* Priest, G.R., and Vogt, B.F., eds., Geology and Geothermal Resources of the Mount Hood Area, Oregon Dep. Geol. Miner. Ind., *Spec. Pap. 14,* 6-15, 1982.

Priest, G.R., M.H. Beeson, M.W. Gannett, and D.A. Berri, Geology, geochemistry, and geothermal reources of the Old Maid Flat area, Oregon: *in* Priest, G.R., and Vogt, B.F., eds., Geology and Geothermal Resources of the Mount Hood Area, Oregon Dep. Geol. Miner. Ind., *Spec. Pap. 14,* 16-30, 1982.

Rutherford, M.J., H. Sigurdsson, S. Carey, and A. Davis, The May 18, 1980 eruption of Mount St. Helens, 1. Melt composition and experimental phase equilibria: *J. Geophys. Res., 90* (B4), 2929-2947, 1985.

Scandone, R., and S.D. Malone, Magma supply, magma discharge and readjustment of the feeding system of Mount St. Helens during 1980: *J. Volcan. Geoth. Res., 23,* 239-262, 1985.

Scheen, W.L., EMMMA, A computer program for three-dimensional modeling of airborne electromagnetic surveys, *in* Proc. Workshop on Modeling of Electrical and Electromagnetic Methods, Lawrence Berkeley Laboratory *Rept. LBL-7053,* 1978.

Stanley, W.D., Tectonic study of Cascade Range and Columbia Plateau in Washington State based upon magnetotelluric soundings: *J. Geophys. Res., 89* (B6), 4447-4460, 1984.

Steele, J.L., D.D. Blackwell, and J.H. Robison, Heat flow in the vicinity of the Mount Hood Volcano, Oregon: *in* Priest, G.R., and Vogt, B.F., eds., Geology and Geothermal Resources of the Mount Hood Area, Oregon Dep. Geol. Miner. Ind., *Spec. Pap. 14,* 31-42, 1982.

Stodt, J.A., G.W. Hohmann, and S.C. Ting, The telluric-magnetotelluric method in two- and three-dimensional environments: *Geophysics, 46* (8), 1137-1147, 1981.

Thayer, T.P., Petrology of the later Tertiary and Quaternary rocks of the north-central Cascade Mountains in Oregon, with notes on similar rocks in Nevada: *Geol. Soc. Am. Bull., 48,* 1611-1652, 1937.

Vozoff, K., The magnetotelluric method in the exploration of sedimentary basins: *Geophysics, 37* (1), 98-141, 1972.

Weaver, C.S., S.M. Green, H.M. Iyer, Seismicity of Mount Hood and structure as determined from teleseismic P wave delay studies: *J. Geophys. Res., 87* (B4), 2782-2792, 1982.

White, C., Geology and geochemistry of Mt. Hood Volcano: *Spec. Pap. 8,* 26 pp., Oreg. Dep. of Geol. and Miner. Ind., Portland, 1980.

White, C.M. and A.R. McBirney, Some quantitative aspects of orogenic volcanism in the Oregon Cascades: *in* Smith, R.B., and Eaton, G.P., eds., Cenozoic Tectonics and Regional Geophysics of the Western Cordillera, *Geol. Soc. Am. Memoir 152,* 51-92, 1978.

Williams, D.L., and T.E.C. Keith, Aeromagnetic and Bouguer gravity maps of the Mount Hood wilderness, Clackamas and Hood River counties, Oregon: U.S. Geol. Survey Misc. Field Investigations *Map MF 1379-D,* scale 1:62,500, 1982.

Williams, D.L., D.A. Hull, H.D. Ackermann, and M.H. Beeson, The Mt. Hood region: Volcanic history, structure, and geothermal energy potential: *J. Geophys. Res., 87* (B4), 2767-2781, 1982.

Wise, W.S., Mount Hood area: *in* Andesite Conf. Guidebook., *Oreg. Dep. Geol. Miner. Ind., Bull, 62,* 81-98, 1968.

Wise, W.S., Geology and petrology of the Mt. Hood area: A study of high Cascade volcanism: *Geol. Soc. Am. Bull, 80,* 969-1006, 1969.

Wollenberg, H.A., R.E. Bowman, H.R. Bowman, and B. Strisower, Geochemical studies of rocks, water, and gases at Mt. Hood, Oregon: Lawrence Berkeley Laboratory *Rept. LBL-7092,* 57p, 1979.

Zoback, M.L., and G.A. Thompson, Basin and Range rifting in northern Nevada: Clues from a mid-Miocene rift and its subsequent offsets: *Geology, 6* (2), 111-116, 1978.

This report was done with support from the Department of Energy. Any conclusions or opinions expressed in this report represent solely those of the author(s) and not necessarily those of The Regents of the University of California, the Lawrence Berkeley Laboratory or the Department of Energy.

Reference to a company or product name does not imply approval or recommendation of the product by the University of California or the U.S. Department of Energy to the exclusion of others that may be suitable.

LAWRENCE BERKELEY LABORATORY
TECHNICAL INFORMATION DEPARTMENT
UNIVERSITY OF CALIFORNIA
BERKELEY, CALIFORNIA 94720